

Journal Pre-proof



A dynamic actin cytoskeleton is required to prevent constitutive VDAC-dependent MAPK-signalling and aberrant lipid homeostasis.

Jack Davis, Thorsten Meyer, Martin Smolnig, Daniel G.J. Smethurst, Lisa Neuhaus, Jonas Heyden, Filomena Broeskamp, Elizabeth S.M. Edrich, Oskar Knittelfelder, Dagmar Kolb, Tobias von der Haar, Campbell W. Gourlay, Patrick Rockenfeller

PII: S2589-0042(23)01616-4

DOI: <https://doi.org/10.1016/j.isci.2023.107539>

Reference: ISCI 107539

To appear in: *ISCIENCE*

Received Date: 23 March 2023

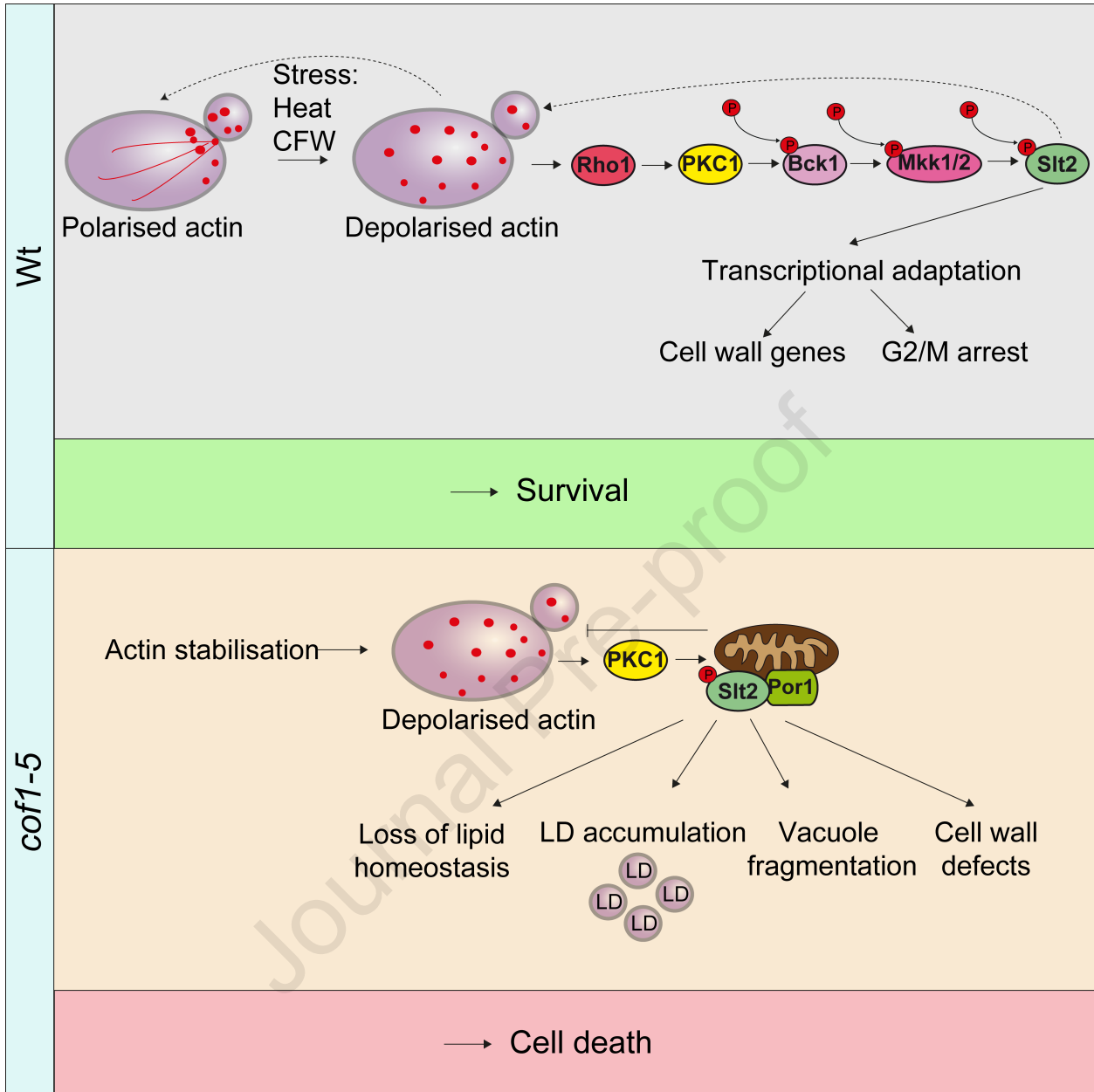
Revised Date: 14 July 2023

Accepted Date: 28 July 2023

Please cite this article as: Davis, J., Meyer, T., Smolnig, M., Smethurst, D.G.J., Neuhaus, L., Heyden, J., Broeskamp, F., Edrich, E.S.M., Knittelfelder, O., Kolb, D., Haar, T.v.d., Gourlay, C.W., Rockenfeller, P., A dynamic actin cytoskeleton is required to prevent constitutive VDAC-dependent MAPK-signalling and aberrant lipid homeostasis., *ISCIENCE* (2023), doi: <https://doi.org/10.1016/j.isci.2023.107539>.

This is a PDF file of an article that has undergone enhancements after acceptance, such as the addition of a cover page and metadata, and formatting for readability, but it is not yet the definitive version of record. This version will undergo additional copyediting, typesetting and review before it is published in its final form, but we are providing this version to give early visibility of the article. Please note that, during the production process, errors may be discovered which could affect the content, and all legal disclaimers that apply to the journal pertain.

© 2023



1 A dynamic actin cytoskeleton is required to prevent constitutive
2 VDAC-dependent MAPK-signalling and aberrant lipid homeostasis.

3 **Authors**

4 Jack Davis^{1§}, Thorsten Meyer^{2§}, Martin Smolnig², Daniel G. J. Smethurst¹, Lisa Neuhaus², Jonas
5 Heyden², Filomena Broeskamp², Elizabeth S. M. Edrich¹, Oskar Knittelfelder³, Dagmar Kolb^{4,5},
6 Tobias von der Haar¹, Campbell W. Gourlay^{1*}, Patrick Rockenfeller^{2*}

7 **Affiliations**

8 ¹Kent Fungal Group, School of Biosciences, University of Kent, Canterbury, Kent, UK.

9 ²Chair of Biochemistry and Molecular Medicine, Center for Biomedical Education and
10 Research (ZBAF), University of Witten/Herdecke (UW/H), Stockumer Str. 10, 58453,
11 Germany

12 ³Max Planck Institute of Molecular Cell Biology and Genetics, Dresden 01307, Germany,
13 Present address: Innovation Campus Berlin, Nuvisan ICB, Berlin 13353, Germany

14 ⁴Medical University of Graz, Core Facility Ultrastructure Analysis, Neue Stiftingtalstraße
15 6/II, 8010 Graz, Austria

16 ⁵Gottfried Schatz Research Center for Cell Signaling, Metabolism and Aging, Division
17 of Cell Biology, Histology and Embryology, Medical University of Graz, Neue
18 Stiftingtalstraße 6/II, 8010 Graz, Austria

19 § These authors contributed equally; * senior authors, these authors contributed equally

20 **Contact Information**

21 Patrick Rockenfeller (Lead contact): Email: Patrick.rockenfeller@uni-wh.de, Phone: +49

22 2302 926 144

23 Campbell Gourlay: Email: Campbell.W.Gourlay@kent.ac.uk; Phone: +44 1227 823535

24 **Summary**

25 The dynamic nature of the actin cytoskeleton is required to coordinate many cellular processes
26 and a loss of its plasticity has been linked to accelerated cell ageing and attenuation of adaptive
27 response mechanisms. Cofilin is an actin-binding protein that controls actin dynamics and has
28 been linked to mitochondrial signalling pathways that control drug resistance and cell death.
29 Here we show that cofilin-driven chronic depolarisation of the actin cytoskeleton activates cell
30 wall integrity MAPK-signalling and disrupts lipid homeostasis in a VDAC-dependent manner.
31 Expression of the *cof1-5* mutation, which reduces the dynamic nature of actin, triggers loss of
32 cell wall integrity, vacuole fragmentation, disruption of lipid homeostasis, lipid droplet (LD)
33 accumulation and the promotion of cell death. The integrity of the actin cytoskeleton is
34 therefore essential to maintain the fidelity of MAPK signalling, lipid homeostasis and cell
35 health in *S. cerevisiae*.

36

37

38 **Introduction**

39 The actin cytoskeleton participates in many cellular processes including cell and organelle
40 architecture, endocytosis, vesicular trafficking, organelle inheritance and communication¹. As
41 a result, the regulation of actin dynamics is essential and is facilitated by accessory proteins that
42 promote rapid assembly and disassembly of filaments. Perturbations in the control of actin
43 dynamics, instigated either through mutations in actin itself, or as a result of the aberrant activity
44 of actin regulatory proteins, have been shown to trigger cell death in a variety of cell types². In
45 many, if not all, of these cases cell death appears to be underpinned by links between the control
46 of actin dynamics and its effects on mitochondrial function. A good example of this lies with
47 the highly conserved actin regulatory protein cofilin. Cofilin is a member of the ADF/cofilin
48 family of small actin binding proteins found in all eukaryotic cells, which are essential for
49 dynamic polymerisation and depolymerisation of actin³. Recent findings suggest that cofilin
50 plays a role in the regulation and maintenance of homeostasis as cells adapt to environmental
51 challenge. For example cofilin has been shown to facilitate the control of permeabilisation of
52 the outer mitochondrial membrane, and so the initiation of apoptosis, in neutrophils at sites of
53 infection in mammalian systems⁴. Cofilin is likely, therefore, to play a major role in innate
54 immune and inflammatory responses. Additionally, aberrant cofilin /actin aggregates, termed
55 ADF/cofilin rods (ACR), which accumulate in normal ageing brains and even more excessively
56 in the hippocampus of Alzheimer's sufferers, are reported to interact with and damage
57 mitochondria under conditions of stress⁵. Cofilin can therefore function within normal cellular
58 responses or, if aberrant, promote disease via its interactions with mitochondria. Subtle changes
59 to the charged surfaces of cofilin have a profound effect on the activity and quality of
60 mitochondrial function. In yeast the regions of cofilin that are involved in controlling
61 mitochondrial function are distinct from the actin binding and regulatory surface⁶. However,

62 despite the mounting evidence that cofilin can control homeostasis and cell fate via
63 mitochondrial regulation, our understanding as to how this is achieved is lacking.

64 Cell death can occur in many different regulated or accidental ways which are characterised by
65 their phenotypic features⁷. Importantly, regulated cell death pathways are not limited to
66 multicellular organisms but also occur in single-cell-organisms such as *S. cerevisiae*^{8,9}. The
67 different modes and subroutines of cell death in yeast, which include accidental, regulated, and
68 programmed forms of cell death, have been classified based on morphological and biochemical
69 criteria¹⁰. Importantly yeast has been successfully used to study lipotoxicity/ lipotoxic cell
70 death¹¹⁻¹⁴.

71 In this project we wished to gain mechanistic insight into the regulation of cofilin/ actin
72 dependent stress signalling and mitochondrial function using the model yeast *S. cerevisiae*. In
73 order to investigate this we made use of the well-characterised *cof1-5* mutant. In this strain two
74 negatively charged amino acid residues are exchanged for alanine (D10A E11A). These amino
75 acid exchanges do not interfere with actin binding *per se* but reduce cofilin's actin
76 depolymerisation efficiency, thus stabilising the actin cytoskeleton¹⁵. We report that cofilin
77 dependent reduction in actin dynamics leads to a number of chronic defects, such as aberrant
78 cell wall construction, vacuole fragmentation and altered lipid metabolism that sensitizes the
79 cells to a necrotic cell fate when they are exposed to additional stress. This "pro-death" cell
80 state is driven by the localisation and constitutive activation of PKC controlled MAPK
81 signalling at the mitochondria.

82 PKC activation of MAPK signalling is essential for yeast cell survival under a range of stress
83 conditions. In addition to its canonical role in PKC/MAPK cell wall integrity the terminal
84 MAPK Slt2 has been shown to phosphorylate several targets involved in responses to
85 environmental challenge. Slt2 therefore has roles in cell wall, oxidative, heat and calcium stress,

86 and functions within cellular processes including cell cycle control, membrane trafficking, actin
87 cytoskeleton organisation¹⁶. Such perturbations to PKC/MAPK signalling are often linked to
88 elevated cell death, highlighting its importance in cell adaption and survival^{17,18}. Given the
89 importance of the PKC/MAPK pathway to survive environmental challenge, cells have
90 developed mechanisms to ensure that its activation is tightly controlled¹⁹. Here we show that a
91 loss of actin regulation can override such controls and leads to the assembly of VDAC/Porin1
92 dependent MAPK signalling at the mitochondrial compartment. Many of the phenotypes
93 associated with *cof1-5* expression could be rescued by the deletion of *POR1*, suggesting a key
94 and previously uncharacterised role for VDAC in MAPK signalling in yeast. In addition, the
95 deletion of genes *LROI* or *DGAI*, that control the accumulation of triglyceride in lipid droplets
96 (LDs) was also sufficient to prevent constitutive MAPK signalling and restore cell health in
97 *cof1-5* mutants.

98 Our data suggests that the integrity of the actin cytoskeleton and the fidelity of PKC/MAPK
99 signalling are inter-connected and that their concerted action is important for cell survival.
100 Actin stabilisation promotes a MAPK signalling module that renders cells vulnerable to
101 environmental challenge. We suggest that this adds to the growing evidence that simple
102 eukaryotes embrace cellular states that ensure cells that cannot respond to environmental cues,
103 such as those with corrupted actin cytoskeleton, are removed from their population.

104

105 **Results**

106 **1. *cof1-5*-induced actin defects and vacuole fragmentation but not mitochondrial** 107 **fragmentation are VDAC-dependent.**

108 In mammalian cells cofilin and its binding partner actin have been shown to interact with the
109 mitochondrial outer membrane pore VDAC^{4,20}. A primary goal of our study was to determine
110 whether phenotypes associated with changes in actin dynamics that are linked to cofilin
111 function are mediated via VDAC in yeast. In order to investigate this we made use of the well-
112 characterised *cof1-5* mutant.

113 During cell division cortical actin patches can be observed to polarise to the growing bud²¹⁻²⁴,
114 however in *cof1-5* cells actin patches are observed throughout the mother and daughter²⁵. We
115 examined whether the actin depolarisation phenotype observed in *cof1-5* cells was
116 VDAC/Porin1 (Por1) dependent by staining the F-actin cytoskeleton with phalloidin-
117 tetramethylrhodamine B-isothiocyanate (phalloidin-TRITC). Surprisingly, the deletion of
118 *POR1* in *cof1-5* cells resulted in a full rescue of the actin-depolarisation phenotype (Fig. 1A,
119 B) and also reverted the cell size increase as observed in *cof1-5* (Fig. 1A, C). These results
120 suggest that the actin defect observed in dividing *cof1-5* cells is not caused by the action of
121 cofilin on actin, but rather by either a loss of regulation that controls actin patch assembly, or
122 the induction of a cellular stress programme capable of triggering actin depolarisation. The
123 rescue of actin depolarisation upon deletion of *POR1* suggests an interaction between cofilin
124 and/or actin with the mitochondrial compartment.

125 A further phenotype associated with *cof1-5*-expressing cells is fragmentation of the
126 mitochondrial network⁶. As the fragmentation of mitochondria has been shown to involve F-
127 actin and cofilin in mammalian cells we considered the possibility that *POR1* deletion in *cof1-*

128 5 cells may also restore mitochondrial morphology. Deletion of *POR1* lead to the accumulation
129 of mitochondria within a single entity (or maximally two) reminiscent of mutations in the ER-
130 mitochondria encountering structure (ERMES), such as *mdm10Δ*, *mdm12Δ*, *mdm34Δ* and
131 *mmm1Δ* (Fig. 1D)²⁶. Mitochondria of *cof1-5 por1Δ* cells also appeared as large spherical
132 structures and identical to those of *por1Δ* (Fig. 1D). As actin has also been linked to vacuole
133 regulation we made use of the fluorescent dye FM4-64 to examine its morphology.
134 Interestingly, *cof1-5* cells showed an aberrant fragmented, or multi-lobed vacuole morphology
135 (Fig. 1E). In *cof1-5* cells 65 % of the cells had multi-lobular vacuoles as compared to only 19
136 % in wildtype (Fig. 1F). Notably, knock out of *POR1* led to a full rescue of this vacuolar
137 phenotype. Additional electron microscopy confirmed the fragmented vacuole phenotype in
138 *cof1-5* cells (Fig. S1). Altogether, these data suggest that the actin depolarisation and vacuole
139 fragmentation phenotypes observed in *cof1-5* cells are Por1-dependent, whereas mitochondrial
140 fragmentation does not share the Por1-dependency.

141

142 **2. The *cof1-5* mutation constitutively activates the cell wall integrity pathway (CWI) in a** 143 **VDAC specific manner.**

144 In addition to changes in growth (Figure 2A) we observed that *cof1-5* mutant cells were prone
145 to flocculation and sedimented rapidly in culture (Figure 2B). Flocculation is a natural
146 phenomenon where cells aggregate in multicellular so-called flocs which increases the chance
147 of survival upon stress²⁷. Flocculation involves remodelling of the cell wall and has recently
148 been connected to cell wall integrity (CWI) signalling²⁸. The fungal cell wall is composed of
149 glucans, chitin, chitosan, mannans, galactomannans and glycoproteins²⁹. Under unstressed
150 conditions chitin is represented at only 2 % of cell wall mass, which can increase up to 20 %
151 upon cell wall stress³⁰. This explains the increased reactivity of yeast cells with the chitin-

152 specific dye Calcofluor White (CFW)³¹ upon cell wall stress. Using CFW staining we could
153 indeed confirm that chitin is enriched at the mutant cell wall as compared to the wildtype (Fig.
154 2C). Examination of the cell wall ultrastructure by electron microscopy revealed that the inner
155 cell wall of the *cof1-5* mutant appeared thicker than in wildtype samples, whereas the electron-
156 dense structures of the outer cell wall were slightly shorter (Fig. 2D). We measured wildtype
157 and mutant cell wall widths and calculated the means for inner- and outer cell walls. Strikingly,
158 we confirmed a substantial increase of inner cell wall width for *cof1-5* (Fig. 2E), whereas the
159 outer cell wall width was slightly reduced (Fig. 2F). Moreover, we observed that these cell wall
160 phenotypes were reversed by additional knock out of *POR1*. These data suggest that VDAC is
161 required for the maintenance of normal cell wall architecture.

162

163 **3. Actin stabilisation changes expression of genes associated with the plasma membrane** 164 **compartment, MAPK signalling and regulation of the cell wall.**

165 The *cof1-5* mutation has been shown to lead to a reduction in the dynamic nature of actin
166 filaments¹⁵. However, as the deletion of *POR1* led to a rescue of the actin patch depolarisation
167 phenotype, we wished to determine whether reduced actin dynamics alone would lead to
168 changes in the cell wall regulation. To achieve this, we made use of a well characterised actin
169 allele, *act1-159*, which reduces actin dynamics by slowing the release of inorganic phosphate
170 following ATP hydrolysis within F-actin filaments³². The expression of *act1-159* led to a
171 significant increase or decrease in the expression of 648 and 141 genes respectively during
172 exponential growth phase (Fig. 3A; Table S1). Genes that were upregulated in response to actin
173 stabilisation could be clustered within several cellular processes by Gene Ontology (Fig. 3B;
174 Table S1). The processes controlling transposition, response to pheromone and cell wall
175 biosynthesis, which are controlled by MAPK pathways, were enriched within the upregulated
8

176 gene data set (Fig. 3B; Table S1). The changes in gene expression related to MAPK signalling
177 in dividing *act1-159* cells were further exemplified by elevated levels of the membrane
178 pheromone receptor *STE2* and the MAPK *FUS3*, which are normally activated by the presence
179 of extracellular pheromone from cells of the opposite mating type. A MAPK involved in
180 signalling in response to cell wall stresses, *SLT2* (also called *MPK1*) and the upstream MAPKK
181 (MKK1) were also upregulated. This was accompanied by the increase in expression of several
182 genes involved in another MAPK controlled process, cell wall biogenesis (Table S1). Within
183 the genes upregulated for cell wall regulation process were those involved in glucan, chitin and
184 mannan regulation as well as genes encoding several GPI anchored proteins (Table S1). To
185 highlight the effects on cell wall we observed that *act1-159* cells exhibited a strong sensitivity
186 to the cell wall stressor Congo Red (Fig. 3C). Overall these data support the finding that actin
187 stabilisation leads to an increase in intracellular stress, a loss of MAPK regulation, which
188 includes CWI activation, and changes in lipid biosynthesis in a manner akin to that observed in
189 *cof1-5* expressing cells.

190

191 **4. *cof1-5* mutation triggers activation of the cell wall integrity (CWI) MAPK pathway.**

192 Our data suggest that cell wall changes observed in *cof1-5* cells are dependent on the presence
193 of VDAC/Por1. As cell wall integrity is managed via MAPK signalling, we sought to determine
194 activation of this pathway in *cof1-5* and *cof1-5 por1Δ* cells by immunoblotting for
195 phosphorylation of the terminal MAPK Slt2 at its amino acid residues T190 and Y192³³. This
196 approach confirmed that Slt2 is constitutively active in *cof1-5* mutant cells and that Slt2
197 phosphorylation is lost upon deletion of *POR1* in both fermentable (glucose) and non-
198 fermentable (glycerol) carbon source containing media (Fig. 4A, B). Constitutive Slt2
199 phosphorylation in *cof1-5* cells was largely reduced by addition of the Pkc1 inhibitor

200 cercosporamide, confirming activation of canonical CWI signalling (Fig. 4C). Expression of
201 *POR1* from a plasmid led to an increase of Slt2 phosphorylation under all tested conditions and
202 was sufficient to compensate for chromosomal loss of *POR1* (Fig. 4D). Unexpectedly, the
203 additional expression of *POR1* from the plasmid on top of basic chromosomal expression in
204 wildtype cells was sufficient to trigger CWI signalling (Fig. 4D). We further used calcofluor
205 white (CFW) stress to trigger CWI signalling. We confirmed Slt2-phosphorylation in response
206 to CFW stress in a concentration dependent manner (Fig. S2 A-C). Basic levels of Slt2-
207 phosphorylation were reduced in *por1* Δ however the strain remained responsive to CFW-
208 induced Slt2-phosphorylation (Fig. S2 D). Since cell wall integrity signalling is a response to
209 stress we wondered whether its activation in *cof1-5* cells was essential to mediate survival upon
210 cell wall stress. We could confirm that while the *cof1-5* mutation led to an increase in the cell
211 population with loss of plasmamembrane integrity, this rose significantly when applying
212 treatment with the Pkc1-inhibitor cercosporamide (Fig. 4E). Combined treatment with CSA and
213 CFW, but not CFW alone, led to a further increase in cells exhibiting plasma membrane
214 permeability in an additive manner, suggesting that Pkc1-activity may promote survival when
215 cofilin/actin-induced stress is experienced. We further tested for cell death sensitivity in a
216 genetic model using gene knock out strains for *POR1* and *SLT2*. In fact, as expected *POR1*
217 deletion provided a rescue from *cof1-5* and CFW-induced cell death, while *SLT2* deletion had
218 the opposite effect (Fig. 4F). In wildtype cells CSA treatment or *SLT2*-deletion increases the
219 PI-positive cell population to 20 %, indicating that under basal conditions the CWI pathway is
220 pro-survival. The *cof1-5* mutant shows increased CWI-signalling and the cell population with
221 loss of plasmamembrane integrity increases concomitantly. It appears that both a loss and gain
222 of Slt2 phosphorylation could result in increased cell death suggesting a non-linear signalling
223 model for Slt2.

224 We further conducted chronological ageing experiments with PI staining and survival plating
225 as two independent readouts for cell death (Fig. 4G, H). Importantly, both readouts suggested
226 that *cof1-5* mediated shortening of the chronological lifespan depends on *POR1*. Welch-
227 ANOVA analysis of survival and PI at day 8 of ageing confirmed a significant reduction in
228 survival and PI-negativity in *cof1-5* cells, which was rescued by *POR1*-deletion (Fig. 4I, J).

229

230 **5. *cof1-5* expression prevents Slt2 localisation to the nucleus and promotes MAPK** 231 **signalling from the mitochondrial compartment.**

232 Using a wildtype strain expressing Slt2-GFP from its endogenous promoter at its original
233 chromosomal locus we confirmed that, in line with earlier analyses of Slt2-GFP localisation³⁴,
234 the majority of cellular Slt2 is found in the nucleus (Fig. 5A, B) However, in a small proportion
235 (5 %) of cells Slt2-GFP could be seen to localise to cytoplasmic foci (Fig. 5A, C). In contrast
236 only 1% of *cof1-5* cells showed Slt2 localisation to the nucleus (Fig 5B), while a significant
237 proportion (30 %) of *cof1-5* cells were observed as having foci (Fig. 5A, C), and the remaining
238 cells showed diffuse green fluorescence throughout the cytosol.

239 Given the porin dependence of the CWI activation in *cof1-5* cells we tested for colocalisation
240 with mitochondria using rhodamine B hexylester. Indeed, the Slt2-GFP foci observed in *cof1-*
241 *5* largely colocalised with rhodamine B hexylester signal after staining (Fig. 5D, E), whereas
242 no colocalisation of Slt2-GFP foci with LDs was detected (Fig. S3A). We next wanted to assess
243 whether mitochondrial Slt2-GFP foci formation was dependent on Por1. For this purpose, we
244 used an Slt2-GFP expression plasmid. The expression from the plasmid showed a similar result
245 as compared to chromosomal expression, but the percentages of cells with Slt2-GFP-foci and
246 nuclear localisation in *cof1-5* were roughly doubled (Fig. 5F-H). We reasoned that this was an
247 effect of Slt2-GFP overexpression from the plasmid used. Importantly, additional deletion of

248 *POR1* reduced the fraction of foci-containing cells in *cof1-5* to wildtype levels while at the
249 same time increasing the percentage of cells with nuclear-Slt2-GFP signal to wildtype levels
250 (Fig. 5F-H). The analysis of Slt2-GFP colocalisation with mitochondria further supports the
251 latter finding in that the Pearson coefficient is reduced to wildtype levels in *cof1-5 por1Δ* (Fig.
252 5I). Additional analysis of Pkc1-GFP showed a similar pattern of foci-formation and
253 colocalization with mitochondria in *cof1-5* as observed when expressing Slt2-GFP (Fig. 5 J-L).
254 The percentage of foci-containing cells was increased by roughly 20 % in *cof1-5* as compared
255 to wild type cells (Fig. 5K) and analysis of the Pearson coefficient of Pkc1 colocalisation with
256 mitochondria was significantly increased from 0.26 to 0.59 (Fig. 5L).
257 Altogether this suggests that activation of MAPK-signalling in *cof1-5* involves Slt2 and Pkc1
258 translocation to mitochondria. This further raises the possibility that Slt2-mediated signalling
259 actively occurs at mitochondria.

260

261 **6. Reduced actin dynamics lead to a Porin-dependent increase in lipid droplet number** 262 **that are required for CWI activation.**

263 Porin has recently been implicated in mitochondrial lipid import³⁵. We therefore determined
264 whether lipid droplet number and their control were altered in *cof1-5* cells. This idea seemed
265 reasonable, since actin and cofilin have been described as regulators of lipid droplet
266 homeostasis in mammalian cells³⁶⁻³⁸. We stained cellular lipid droplets of wt and *cof1-5*
267 mutants having additional gene-knock-out-deletions encoding for the acyltransferases Lro1 and
268 Dga1 using the specific BODIPY 493/503 dye. Lipid droplets of *cof1-5* cells were more
269 abundant than in wildtype cells (Fig. 6A, B). Interestingly, this increase in lipid droplet number
270 was reverted when *LRO1* or *DGAI*, or both in combination, were knocked out in *cof1-5* cells
271 (Fig. 6A and Fig 6B). Basic levels of Slt2-phosphorylation were significantly decreased in
12

272 *lro1Δ* and *lro1Δ dga1Δ* DKO phenocopying *por1Δ* (Fig. S4A, B). In addition to that a non-
273 significant trend in reduced susceptibility to CFW treatment was noted (Fig. S4A, B). We
274 further found that the increase in lipid droplet number in *cof1-5* cells was reversed upon deletion
275 of *POR1* or *SLT2* (Fig. 6C, D, S4C). Electron microscopy further supported the hypothesis that
276 LD number is increased in *cof1-5* (Fig. 6E) and as a response to CFW treatment (Fig. S4D).
277 Some LDs as observed in CFW treated cells appear to be surrounded by a membrane (Fig.
278 S4D). Usually the membranes surrounding LDs identify as ER membranes³⁹, which may
279 suggest an increase of LD-ER-membrane contacts.

280

281 **7. The acyltransferases Lro1 and Dga1 are required for MAPK-related changes in *cof1-*** 282 **5.**

283 Given these findings we also investigated whether lipid droplet regulation at the stage of fatty
284 acid esterification, via Lro1 and Dga1, would affect CWI signalling or other downstream effects
285 in *cof1-5*. Actin depolarisation as observed in *cof1-5* could neither be rescued by *LRO1*- or
286 *DGA1*-single-KOs, nor by the double knock out, both of which genes encode for
287 acyltransferases (Fig. 7A). However, the growth defect (Fig. 7B) and the flocculation
288 phenotypes (Fig. 7C) of *cof1-5* were compensated by knock-out of either *LRO1* or *DGA1*. As
289 expected by the rescue of flocculation, the constitutive phosphorylation of Slt2 observed in
290 *cof1-5* cells was turned off upon deletion of *LRO1* or *DGA1* (Fig. 7D). We next tested whether
291 diverse stresses such as hydrogen peroxide (H₂O₂), heat, CuSO₄ or calcofluor white (CFW)
292 affected LD abundance. Interestingly, all the stresses triggered an increase in LD abundance
293 with the cell wall stress applied through CFW treatment being strongest (Fig. 7E). In summary,
294 this suggests an active role of CWI-signalling in the control of lipid metabolism and LD
295 homeostasis downstream or independent of cofilin-mediated actin regulation.

296

297 **8. Cofilin and Porin are important regulators of lipid homeostasis**

298 With the Porin-dependent changes in lipid droplet quantity as observed in *cof1-5* cells we
299 sought to characterise its effects on global lipid homeostasis. We detected significant changes
300 in *cof1-5* cells for PC, PS, TG (Fig. 8A), PA, PG, lyso-PI (LPI), ceramide (Fig. 8B), sterol
301 esters (SE) and ergosterol (Erg) (Fig. 8C), and the complex sphingolipids MIP2C and MIPC
302 (Fig. 8D) when we compared shotgun lipidomic profiles to wild type (additional data on lipid
303 species are available in Fig. S5 A-E). In all cases, with the exception of LPI, all lipid class levels
304 were restored to wild type levels upon deletion of *POR1*, highlighting the significance of this
305 mitochondrial protein for lipid regulation. The most prominent decrease in *cof1-5* cells was
306 observed for TG. However, additional high performance thin layer chromatography (HPTLC)
307 measurements could only confirm a trend in decrease due to strong variation upon the
308 individual samples (Fig. 8E). The strongest increases were observed for PA, LPI, sterolesters
309 and ergosterol as well as the complex sphingolipids MIP2C and MIPC. The increases in SE and
310 Erg in *cof1-5* as well as the reduction by the additional gene KOs were confirmed by additional
311 HPTLC quantification and can thus be considered as robust (Fig. 8F, G). Since the neutral lipids
312 (SE and TG) are stored in LDs we reasoned that the ratio of SE to TG might correlate with the
313 LD phenotype as observed before. We thus calculated the SE/TG index ($i_{SE/TG}$) and confirmed
314 significant change of the index in *cof1-5* (Fig. 8H) which correlates with the increased amount
315 of LDs as quantified in Fig. 6A-D. Interestingly, gene KOs of *POR1*, *DGAI*, *LRO1* and *SLT2*
316 revert $i_{SE/TG}$ back to wildtype levels. Further to this, we noted significant lipidomic changes in
317 the *POR1* deletion strain itself (e.g. PC, TG, PA, Cer, CL, Fig. 8A, B) which confirms that Por1
318 indeed has crucial impact on total lipid homeostasis.

319 In summary, these results give evidence that lipidomic changes in *cof1-5* depend on Por1 and
320 further suggest that lipidomic changes in *cof1-5* could be causally linked to CWI signalling.

321

Journal Pre-proof

322 Discussion

323 In a healthy dividing yeast cell the experience of a stressor that perturbs the cell wall results in
324 the depolymerisation of the F-actin cytoskeleton, this is required to assist in both cell cycle
325 arrest (G2/M) and the activation of the cell wall integrity pathway³⁰. We have shown that cells
326 expressing the *cof1-5* mutation, which leads to the chronic depolarisation of F-actin patches,
327 exhibit hallmarks of constitutive Pkc1/Slt2 activation, such as flocculation and vacuole
328 fragmentation. Our data also show that this aberrant PKC/Slt2 signalling depends on the
329 mitochondrial outer membrane protein Por1, which is the yeast orthologue of mammalian
330 voltage dependent anion channel (VDAC). Por1 is known to form a pore in the outer
331 mitochondrial membrane thereby facilitating metabolic flux from mitochondria to the cytosol
332 and vice versa^{35,40}. Por1 further has been implicated in the control of cell death in response to
333 stress in previous studies^{41,42}. However VDAC has also been shown to participate in other
334 cellular processes including the regulation of lipid traffic³⁵ and in AMPK/Snf1 signalling⁴³⁻⁴⁵.
335 Here we show that the actin cytoskeleton and mitochondria coordinate MAPK signalling
336 through VDAC and that this plays a role in cell fate. One possibility is the existence of a
337 physical interaction, as was shown in the case of AMPK/Snf1 signalling⁴⁴, whereby Slt2
338 relocates from the nucleus to the mitochondria and docks with VDAC to elicit an alternate
339 signalling response that promotes cell death. In line with this we did observe that the deletion
340 of *POR1* prevented constitutive activation of Slt2 in *cof1-5* cells restored its localisation to the
341 nucleus and reduced the necrotic cell population. Despite a clear correlation between the
342 prevention of Slt2 activation in *cof1-5* cells by deletion of *POR1*, which led to apparent
343 improvement in cell health, we observed the opposite effect when cells were treated with the
344 PKC inhibitor CSA. This result, while unexpected, may be explained by additional off target

345 effects of CSA, or indeed as a result of functions of PKC that lie outside of the canonical
346 PKC/Slr2 cell wall integrity signalling system. Additional evidence to support a direct link from
347 VDAC to Slr2 activation comes from our finding that the overexpression of *POR1* was also
348 sufficient to activate Slr2. Connections between mitochondria and MAPK signalling are
349 emerging, for example a recent study demonstrated mitochondrial participation in MAPK
350 signalling regulating proteasome granule formation upon carbon starvation⁴⁶.

351 A number of lipid classes were found to show significant change in the *cof1-5* mutant. These
352 included PC, PS, and TG, PA, PG, LPI, ceramide, sterol esters (SE), ergosterol (Erg) and the
353 complex sphingolipids MIP2C and MIPC (Fig. 8A-D). These changes were largely reversed
354 when *POR1* was knocked out suggesting a clear role for VDAC in the control of lipid
355 homeostasis, possibly via the activation of Slr2. The overall increase in PA might also account
356 for the changes in mitochondrial morphology as this phospholipid has been shown to regulate
357 mitochondrial fusion via control of Ugo1 biogenesis⁴⁷. Mitochondrial phospholipids such as
358 PG and CL have been connected to Pkc1/CWI signalling^{48,49}. Loss of CL has also been shown
359 to impair CWI signalling which led to defective mitophagy⁵⁰. We also detected changes in the
360 lipid profile of *POR1*-deleted cells as such, which is in line with recently published findings
361 ^{35,51,52}. This raises the possibility that actin triggers changes in lipid homeostasis with Porin
362 acting as a central point of lipid flux control, or indeed as a component of the signalling system
363 that regulates lipid homeostasis itself. Interestingly the ER-mitochondria encountering structure
364 (ERMES), which can facilitate lipid exchange between these compartments, has been
365 implicated in cell death^{53,54}.

366 Our lipidomic results further support the notion that *por1Δ* phenocopies *pgs1Δ*. Pgs1 catalyses
367 the first step of mitochondrial CL synthesis, which is the phosphorylation of
368 phosphatidylglycerol. *pgs1Δ* has reduced levels of beta-1,3-glucans in its cell wall which is thus

369 defective⁵⁵. Por1 and Por2 have recently been suggested to mediate mitochondrial phospholipid
370 import succumbing to PG and CL synthesis³⁵. Our data are in line with these findings and
371 further support the idea of Por1 as a regulator of mitochondrial phospholipid import.

372
373 Intriguingly, we found that two acyltransferases Dgal and Lro1 were also essential for
374 activation of Slt2 and all the downstream phenotypes with the exception of actin
375 depolymerisation. Given the changes of LD abundance that we observed upon cell wall stress
376 and found in *cof1-5* expressing cells this suggests that CWI signalling involves lipidomic
377 rearrangements and dynamic changes of cellular lipid droplets. Interestingly, the inhibition of
378 actin dynamics through *COF1* depletion has also been shown to disrupt adipogenesis and lipid
379 storage in 3T3-L1 cells³⁸.

380
381 Our findings that actin and mitochondrial functions are linked to lipid homeostasis in yeast may
382 have relevance for antifungal resistance. Mitochondrial function has been linked to changes in
383 cell wall function and to changes in azole sensitivity, a class of drugs that target ergosterol
384 synthesis⁵⁶. Ergosterol-levels are controlled under normal conditions, but conditions of stress
385 (e.g. osmotic or cell wall stress) can require rapid change in ergosterol content. A significant
386 increase in ergosterolesters was observed in *cof1-5* cells (Fig. 8C, F), suggesting that these cells
387 are dealing with an ergosterol overflow, thus detoxifying through esterification and storage in
388 LDs. LDs accumulate upon cell wall stress in *cof1-5* cells and in wildtype cells upon CFW
389 stress, where LDs appear to have strong contacts with ER-membranes (Fig. 6, S4). One
390 possibility is that actin and cofilin are needed to facilitate non-vesicular sterol transport by Osh
391 and Lam proteins⁵⁷⁻⁵⁹. Another possibility is that, through activation of the CWI pathway, Pkc1
392 can phosphorylate Pah1^{60,61} (which dephosphorylates PA to yield diacylglycerol) leading to its
18

393 degradation by the proteasome⁶². This in turn would increase PA levels and decrease TG at the
394 same time which is what we observe in *cof1-5* expressing cells. Of note, deletion of *pah1* has
395 been described to shorten chronological lifespan⁶³, which suggests a pro-death trigger upon loss
396 of Pah1 function. Since Pah1 activity has been described to be essential for homotypic vacuole
397 fusion⁶⁴, this also offers an explanation for the fragmented vacuole phenotype as we observed
398 in *cof1-5* cells. Indeed, the fragmented vacuoles of *cof1-5* look very similar to vacuoles as
399 observed in *pah1*Δ or propranolol-treated cells, which represents a pharmacological treatment
400 to inhibit Pah1-activity⁶⁴. The increase in ergosterol as well as the increase in complex
401 sphingolipids observed in *cof1-5* expressing cells may represent an adaptation to overcome
402 mechanical stress at the plasma membrane. Generally the integration of complex sphingolipids
403 together with sterols results in increased packaging and thus higher density which renders the
404 plasma membrane more resistant to mechanical stress⁶⁵. Thus, the activation of Slt2 in actin
405 stabilised cells may contribute to the cell's response to stress and so survival in the short term.
406 However, as such cells are clearly sensitive to additional stress, we favour an interpretation that
407 chronic actin depolymerisation in dividing cells promotes necrotic cell death.

408 Permeabilisation of the vacuole is a feature of regulated cell death in yeast, which through
409 vacuolar release of Pep4, an orthologue of human cathepsin D, into the cytosol succumbs to
410 cell death⁶⁶⁻⁶⁸. More recently a molecular pathway of how vacuole membrane permeabilisation
411 is established in yeast was proposed⁶⁹. The vacuolar phenotype as observed in *cof1-5* cells in
412 our study might have similarity to the previously described cell death routines but additionally
413 involves mitochondrial Por1 activity and lipid metabolism. Further investigation will be
414 required to test this possibility.

415 In summary, our study provides further evidence that the regulation of actin dynamics is crucial
416 for cell fate determination. We show that a reduced ability to regulate actin in dividing yeast

417 cells leads to a pro-death mode of MAPK signalling under conditions of stress. We would argue
418 that this represents a mechanism by which cells that are unable to regulate actin may be lost
419 within a population of cells, such as a colony or biofilm, and postulate that this may represent
420 a novel cell death mechanism in yeast that helps ensure clonal integrity.

421 **Limitations of the Study**

422 The authors recognise that this study opens a number of questions that arise as a consequence
423 of unrecognised interplay between lipid homeostasis, membrane organisation and cell
424 signalling systems in yeast. Further investigations that we suggest within the discussion section
425 highlight a current need to improve our understanding of lipid regulation within eukaryotic
426 cells. A further limitation lies within our current understanding of yeast cell death as a regulated
427 process. Although there is strong evidence to suggest that different modes of death exist, the
428 experimental tools available to differentiate between programmed and passive cell death in
429 yeast are, in the authors view, limited at time of writing. This led to a conservative interpretation
430 of the data presented as a loss of cellular integrity as opposed to a mechanism of regulated cell
431 death.

432 **Acknowledgements**

433 We thank Pekka Lappalainen and David Drubin for providing the *cof1-5* and *act1-159* mutant
434 strains. The pRS426-SLT2-GFP plasmid was a kind gift from Matthias Peter and pYX122-
435 mtGFP from Benedikt Westermann. We are thankful to Dominique Pernitsch and Kerstin
436 Hingerl for technical assistance in electron microscopy. P.R. and CWG were supported by the
437 Erwin Schrödinger Fellowship from the Austrian Science Fund (FWF) (J3742-B28) and the

438 University of Kent. P.R is supported by the “NRW Rückkehr Programm” from the Ministry of
439 Culture and Science of the German State of North Rhine-Westphalia”.

440 **Author contributions**

441 Conceptualisation, C.W.G., and P.R.; Methodology, J.D., T.M., M.S., D.S., L.N., J.H., F.B.,
442 E.S.M.E., O.K., D.G., T.vd.H, C.W.G. and P.R.; Validation, J.D., T.M., M.S., O.K., C.W.G.
443 and P.R.; Formal Analysis, J.D., T.M., M.S., O.K., and P.R.; Investigation, J.D., T.M., M.S.,
444 D.S., L.N., J.H., F.B., E.S.M.E., O.K., and P.R.; Data Curation, P.R.; Writing-Original Draft
445 Preparation, C.W.G., and P.R.; Writing-Review and Editing, J.D., T.M., M.S., O.K.; Figure
446 Visualisation, C.W.G. and P.R.; Supervision, Project Administration, and Funding Acquisition,
447 C.W.G. and P.R. All authors have read and agreed to the published version of the manuscript.

448

449 **Declaration of Interests**

450 The authors declare no competing interests

451

452 **Inclusion and Diversity**

453 We support inclusive, diverse, and equitable conduct of research.

454

455

Figure Titles and Legends

Graphical abstract. Schematic view of VDAC-dependent MAPK signaling. The actin cytoskeleton of wildtype yeast cells is polarised along the mother-bud axis. Upon cell wall stress such as heat or calcofluor white (CFW) administration the cytoskeleton depolarizes and the CWI MAPK signaling pathway is triggered involving Rho1, Pkc1, Bck1, Mkk1/2 and Slk2. This leads to transcriptional adaptation of cell wall genes and G2/M arrest and has pro-survival character. In *cof1-5* cells actin is stabilised and chronically depolarised. Chronic depolarisation of actin constantly triggers the CWI pathway with its main players Pkc1 and Slk2 localising to the mitochondrion in a Por1-dependent fashion. This leads to cell wall defects, vacuole fragmentation, loss of lipid homeostasis, LD accumulation and finally culminates in cell death.

Figure 1. *cof1-5*-induced actin depolarisation but not mitochondrial fragmentation are VDAC dependent. (A, B) Actin phalloidin (red) and DAPI (blue) staining at exponential growth phase (6h) reveals depolarised actin cytoskeleton in the *cof1-5* mutant, which is rescued by additional *POR1* deletion. Representative microscopy pictures are shown in (A) and cells with polarised actin were quantified in (B). (C) *cof1-5* cells have an increased mean cell diameter (as determined with a CASY cell counter). (D) Fluorescence microscopy pictures at exponential growth phase of wt and *cof1-5* with and without additional *POR1* deletion expressing mitochondrial GFP from a plasmid (pVT100U-mt GFP). (E, F) *cof1-5* mutation leads to Por1-dependent vacuole fragmentation as visualised by FM4-64 staining. Representative microscopy images are shown in (E) and a quantification of cells containing multi-lobular vacuoles is depicted in (F). Statistical significance in (B) (C) and (F) was assessed using ordinary one-way ANOVA. See also Fig. S1.

479

480 **Figure 2. *cof1-5* mutation triggers growth defect, flocculation, and cell wall alterations,**
481 **which depend on *POR1*.** (A) Growth performance in liquid culture is reduced in *cof1-5* as
482 compared to wildtype (Wt) but is restored by additional *POR1* deletion. (B) Cultures bearing
483 the *cof1-5* mutation sediment quickly when shaking is stopped (flocculation phenotype).
484 Additional *POR1* deletion prevents flocculation in *cof1-5*. (C) Calcofluor white staining
485 detecting chitin exposure at the cell wall confirms flocculation phenotype of *cof1-5* cells. (D,
486 E, F) The cell wall was analysed by electron microscopy. *cof1-5* mutation is associated with a
487 thicker inner cell wall and thinner outer cell wall. EM-micrographs are shown in D and
488 quantifications of the inner and outer cell wall are plotted in E and F, respectively. ICW, inner
489 cell wall; OCW, outer cell wall; LD, lipid droplet. Statistical significance in (E) was assessed
490 using Kruskal-Wallis test and in (F) Welch ANOVA was performed.

491

492 **Figure 3. Transcriptional changes in the actin mutant *act1-159* suggest involvement of**
493 **MAPK signalling, flocculation and lipid metabolism.** (A) Transcriptional changes of *act1-*
494 *159* vs. *ACT1* cells grown to log phase in YPD media were investigated by microarray and
495 plotted in a volcano plot. Gene ontology analysis for the GO-term PROCESS was completed
496 using the GO SLIM mapper function available on the *Saccharomyces cerevisiae* genome
497 database⁷⁰ and upregulated genes clustered within enriched cellular processes are depicted in
498 panel (B). (C) Congo red sensitivity of wild type and *act1-159* mutant cells was assessed by a
499 spotting assay using a ten-fold serial dilution series from a starting cell number of 2×10^5 . See
500 also Table S1.

501 **Figure 4. *cof1-5* mutation triggers activation of the CWI pathway.** (A, B) Immunoblots
502 detecting Slt2 phosphorylation when grown on glucose and glycerol containing media are
23

503 shown in A and B, respectively. (C) Pkc1 inhibition by cercosporamide (CSA) administration
504 prevented Slr2 phosphorylation. (D) Porin deletion and overexpression reveal dependence of
505 Slr2 phosphorylation on Por1. (E) *cof1-5* mutation triggers loss of plasmamembrane integrity,
506 as assessed flow cytometrically with PI-positivity at 48 h after inoculation. PI-positivity is
507 exacerbated by additional Pkc1 inhibition using the Pkc1-inhibitor cercosporamide or applying
508 additional cell wall stress with calcofluor white (CFW). Combined treatment with CSA and
509 CFW at the same time shows additive effects. (F) *POR1* deletion rescues from *cof1-5*-
510 dependent loss of viability and loss of plasmamembrane integrity, whereas *SLT2* deletion
511 sensitises to cell death. (G-J) Chronological ageing analysis reveals shortening of chronological
512 lifespan in *cof1-5* cells which depends on *POR1*. Colony forming unit formation based on
513 clonogenic survival is depicted in G and H, whereas PI positivity is shown in I and J. Statistical
514 significance in E, F, H and J was assessed using Brown-Forsythe and Welch-ANOVA test.
515 Asterisks indicate significance based on p-levels of the comparisons to the respective control
516 strains. See also Fig. S2.

517

518 **Figure 5. Slr2 localisation to the mitochondrial compartment is enhanced in *cof1-5* cells.**

519 (A) Slr2, which is mostly found in the nucleus in wildtype cells at stationary phase, forms
520 punctate foci in *cof1-5*, as documented by fluorescence microscopy using chromosomally
521 tagged SLT2-GFP under control of its endogenous promoter. Deconvolved pictures with
522 Hoechst staining for nuclei are shown. (B, C) Cells showing nuclear localisation of Slr2-GFP
523 (B) and foci-forming cells (C) were quantified, plotted and analysed for significant localisation
524 change as compared to wildtype. (D) Representative fluorescence microscopy pictures of Slr2-
525 GFP expressing cells with rhodamine B hexylester staining for colocalization analysis with
526 mitochondria. (E) Colocalisation of Slr2-GFP (green) with the mitochondrial stain rhodamine

527 B hexylester was increased in *cof1-5* as shown by significant increase of the Pearson
528 colocalisation coefficient. (F-I) Slt2-GFP expression from a plasmid was used to monitor
529 cellular Slt2 localisation in *cof1-5* cells in dependence of *POR1*. Representative microscopy
530 pictures are shown in (F), Slt-GFP-foci-containing cells are quantified in (G), cells with nuclear
531 Slt2 are quantified in (H) and the Pearson coefficient of Slt2-GFP colocalization with
532 mitochondria is visualised in (I). (J, K) Expression of Pkc1-GFP under control of its
533 endogenous promoter reveals increased PKC1-GFP foci formation in *cof1-5* (J, K).
534 Representative fluorescence microscopy pictures of individual Pkc1-GFP expressing cells with
535 additional rhodamine-B-hexylester staining for mitochondria and autodot staining for LDs are
536 shown in (J) and cells with Pkc1-GFP foci are quantified in (K). (L) The Pearson coefficient
537 was determined as a measure of colocalisation of Pkc1-GFP with mitochondria (rhodamine-B-
538 hexylester). Statistical significance in (B) and (C) was assessed using Welch's t test, (E, K, L)
539 were analysed using unpaired t test and (G, H, I) by ordinary one-way ANOVA. See also Fig.
540 S3.

541
542 **Figure 6. Reduced actin dynamics lead to a porin-dependent increase in lipid droplet**
543 **number that are required for CWI activation.** (A, B) Increase of LD number in *cof1-5*
544 depends on Lro1 and Dga1. Mean LD-numbers per cell are plotted in (A) and representative
545 microscopy pictures are shown in (B). Each dot in (A) represents the mean LD number per cell
546 of a single experiment (n=6) with at least 119 cells being evaluated per experiment. (C, D) Gene
547 deletions of *POR1* or *SLT2* are sufficient to prevent LD accumulation in *cof1-5*. Mean LD
548 numbers per cell were assessed by quantifying fluorescence microscopy pictures using Bodipy
549 staining (C). Representative fluorescence microscopy images are shown in (D). (E)
550 Representative EM micrographs supporting the observation of LD-number-increase in *cof1-5*.

25

551 V, vacuole; LD, lipid droplet; N, nucleus. Statistical significance in (A) and (C) was assessed
552 using 2-way-ANOVA with *cof1-5* mutation as first factor and additional KO as second factor.
553 See also Fig. S4.

554

555 **Figure 7. The acyltransferases Lro1 and Dga1 are required for MAPK-related changes in**
556 ***cof1-5*.** (A) Polarisation of the actin cytoskeleton was assessed using phalloidin (red) and DAPI
557 (blue) staining. The *cof1-5* mutant shows loss of actin polarisation, which is not rescued by
558 gene KO of *LRO1*, *DGA1* or a combined double deletion of the ladder. (B, C) The growth defect
559 (B) and flocculation phenotype (C) as observed in *cof1-5* are restored by additional deletion of
560 the acyltransferases *LRO1*, *DGA1*, or in the double deletion mutant (*lro1Δ dga1Δ*). (D) Slt2
561 phosphorylation in *cof1-5* depends on Lro1 and Dga1 as the KO of either corresponding gene
562 and the double KO prevents Slt2 phosphorylation. (E) Mean LD abundance per cell was
563 quantified in diverse conditions of stress. 150 cells per condition and experiment were
564 quantified with a total of three independent experiments (n=3). Statistical significance in (E)
565 was assessed using ordinary one-way ANOVA.

566

567 **Figure 8. Lipidomic analysis reveals characteristic Por1-dependent changes in the lipid**
568 **profile of *cof1-5*.** (A, B) Mass spectrometry-assisted lipidomic quantification of highly
569 abundant (A) and less abundant yeast lipids from total cell extracts (B). (C, D) Sterolesters and
570 free ergosterol were quantified separately as shown in (C) and sphingolipids are depicted in
571 (D). (E-H) Lipidomic changes in the neutral lipid classes TG (E), SE (F), Erg (G) and the
572 $\text{index}_{\text{SE/TG}}$ (H) were further verified by additional HPTLC analysis. Statistical significance in
573 (A-G) was assessed using two-way ANOVA with *cof1-5* mutation as first factor and additional

- 574 KO as second factor, except for CL, LPC and LPE in (B), which were analysed using Kruskal
575 Wallis test; (H) was analysed by Brown-Forsythe and Welch ANOVA test. See also Fig. S5.

Journal Pre-proof

576 **STAR Methods**

577

578 **RESOURCE AVAILABILITY**

579

580 **Lead contact**

581 Further information and requests for resources and reagents should be directed to and will be
582 fulfilled by the lead contact Patrick Rockenfeller (Patrick.rockenfeller@uni-wh.de) and
583 Campbell Gourlay (C.W.Gourlay@Kent.ac.uk).

584

585 **Materials availability**

586 Plasmids and yeast strains generated in this study are available upon request.

587

588 **Data and code availability**

- 589
- Microarray data, original western blot images, lipidomics data and Prism files have been
590 deposited at Mendeley and are publicly available as of the date of publication. doi:
591 10.17632/bgkscw9ns9.1. Microscopy data reported in this paper will be shared by the
592 lead contacts upon request.
 - This paper does not report original code.
 - Any additional information required to reanalyse the data reported in this paper is
595 available from the lead contacts upon request.

596

597 **EXPERIMENTAL MODEL**

598 All experiments (except Fig. 3) were carried out using the wildtype (Mata *ura3-52 his3Δ200*
599 *leu2-3,112 lys2-801 ade2-101 COF1::LEU2*) and *cof1-5* mutant (Mata *ura3-52 his3Δ200 leu2-*
600 *3,112 lys2-801 ade2-101 cof1-5::LEU2*) *S. cerevisiae* strains as generated and described by
601 Lappalainen et al.¹⁵. Additional gene-knock outs in these two strains for *LRO1* and *DGA1* were
602 generated using the Cre-LoxP system with the KanMX marker for selection⁷¹ using the primers
603 as listed in the key resource table. The *lro1Δ dga1Δ* double knock out was generated based on
604 the *dga1::kanMX* single knock out strain using the pFA6a-Ura3-cassette⁷² for the additional
605 LRO1 knock out. POR1-, and SLT2-gene knock outs were generated according to the protocols
606 and primer design of Janke et al.⁷³ using the pFA6a-KanMX6-cassette⁷⁴. See KRT for primer
607 sequences.

608 For the experiments shown in Fig. 3 the *act1-159* mutant (MATa *act1-159::HIS3 his3D200*
609 *tub2-101 ura3-52 leu2-3, 112*) which harbours the V159N mutation and has reduced actin
610 dynamics was used together with its corresponding wildtype control strain (MATa *ACT1::HIS3*
611 *his3D200 tub2-101 ura3-52 leu2-3, 112*)³².

612
613 Plasmids were propagated in *E. coli* K12 DH5α (see key resource table for details). *POR1* was
614 cloned into pAG416GPD CEN URA by gateway-cloning⁷⁵ using pDONR221-*POR1* as a
615 donor-plasmid. pYX122-mtGFP was obtained from Benedikt Westermann⁷⁶. The *SLT2*-GFP
616 expression plasmid was obtained from Matthias Peter.

617 Slt2-EGFP as shown in Fig. 5A and Pkc1-EGFP as shown in Fig. 5J was expressed under
618 control of their endogenous promoters at their original loci. These strains were generated by
619 PCR and homologous recombination according to established protocols⁷³ using the plasmid
620 pYM27 and primers as listed in the KRT, except for the experiment shown in Fig. 5F-I, where
621 Slt2-GFP was expressed from a plasmid pRS426-SLT2-GFP³⁴. Transformation of yeast cells
29

622 with plasmids or linear DNA for homologous recombination was performed using the lithium
623 acetate method⁷⁷. At least three different clones were tested to rule out clonogenic variations.
624 All experiments (except for ageing experiments as shown in Fig. 4G-J) were carried out in yeast
625 peptone medium with glucose (YPD). YPD medium contains 1% yeast extract (BD), 2%
626 peptone (BD), and 2% glucose. Synthetic complete medium with glucose without Uracil (SCD-
627 Ura), was only used when selection was required for strain construction or to maintain selection
628 for plasmids. SC medium contains 0.17% yeast nitrogen base (Difco), 0.5% (NH₄)₂SO₄, and 30
629 mg/L of all amino acids (except 80 mg/L histidine and 200 mg/L leucine), 320 mg/L uracil, 30
630 mg/L adenine, and 2% glucose. All media were prepared with ultrapure water (MilliQ) and
631 subsequently autoclaved (20 min, 121 °C, 110 kPa). Amino acid mixtures and glucose were
632 sterilised separately as 10× stocks and added after autoclaving. All yeast cultures were
633 inoculated from a stationary overnight culture to an OD₆₀₀ = 0.1 and then grown at 30 °C and
634 145 rpm shaking for indicated time points.

635

636 METHOD DETAILS

637

638 **Growth Assays**

639 Strains were inoculated from stationary overnight cultures to an OD₆₀₀ of 0.1 in 24-well plates
640 (Sarstedt, 1 ml total volume per well) in two or three independent experiments, each containing
641 at least three biological replicates. The plate was automatically measured for 24–48 h using a
642 BMG LabTech SPECTROstar^{Nano} plate reader with double orbital shaking at 400 rpm and 30
643 °C, with OD₆₀₀ measurements every 30 min. Growth curves were plotted in GraphPad Prism.

644

645 **Analysis of cell viability, density and diameter**

30

646 Propidium iodide (PI) staining was used to determine loss of membrane integrity^{78,79}. Cells
647 were harvested in 96-well plates at indicated time points and resuspended in 250 μ L of 100
648 μ g/L PI in PBS, and incubated in the dark for 10 min at room temperature. After incubation,
649 cells were washed once with 250 μ L PBS and analysed via flow cytometry (Beckmann Coulter
650 Cytoflex). A total of 30,000 cells per strain and condition were measured and analysed with
651 CytExpert software. For calcofluor white (CFW) stress experiment in Fig. 4E, wt and *cof1-5*
652 cells were grown overnight and inoculated to an OD₆₀₀ of 0.1, then grown at 30°C. After 22 h
653 of growth, cells were subjected to either 100 μ M cercosporamide, 200 μ M CFW or both, and
654 allowed to grow for further 26 h. CFW stress at 200 μ M as shown in Fig. 4F and Fig. S4A, B
655 was carried out at exponential growth phase (six hours after inoculation to an OD₆₀₀ of 0.1) and
656 PI was detected 18 hours after stress. For chronological ageing analysis cultures were
657 inoculated to an OD₆₀₀ of 0.1 in SCD medium as mentioned above with additional
658 supplementation of 90 mg/ L lysine (+3x), 10 g/ L myo-inositol (55 μ M), and 97.8 mg/ L
659 adenine. Samples were measured at indicated days of ageing by clonogenic survival plating and
660 PI staining to determine viability.

661 For clonogenic survival plating serial dilutions of the main cultures were used to measure cell
662 densities using a CASY cell counter essentially as described before¹². As an adaptation to
663 former protocols the serial dilutions of all strains were made using ddH₂O containing 10 mM
664 EDTA. The addition of EDTA avoided cell aggregation, which is a characteristic of *cof1-5*
665 cells. Without EDTA treatment reliable estimation of living cells by counting of colony forming
666 units (CFU) was impossible.

667 Mean cell diameters were determined based on measurement with a CASY cell counter, which
668 calculates mean cell size based on electric current shifts which are due to the cells acting as
669 electric isolators in conducting salt solution. For these measurements the complex cell mixtures

670 containing cells at all replicative stages were used, which includes single mother cells, bud-
671 containing mother cells and single daughter cells.

672

673 **Fluorescence microscopy**

674 *S. cerevisiae* strains were inoculated to an $OD_{600} = 0.1$ from overnight cultures in YPD medium
675 and harvested at 6h after inoculation for analysis at exponential growth phase or 24h for
676 analysis at stationary phase. Cells were immobilised on microscopy slides containing 2%
677 agarose⁸⁰. Fluorescence was detected using a Nikon Eclipse Ni-U fluorescence microscope with
678 a Hamamatsu Orca-Spark C11440-36U monochromatic camera and Nikon Intensilight C-HGFI
679 illumination system. Fluorescence images were captured and saved as z-stacks in a range of 5
680 μm with 200 nm steps using NIS-Elements BR 4.13.05 64-bit with N-dimensional acquisition.
681 Deconvolution and colocalisation analysis was performed with Huygens essential 21.10
682 software. Further processing such as maximum intensity z-projection, brightness/contrast
683 adaptation, scale bar inclusion, colour merging was performed in Fiji/ ImageJ⁸¹.

684 Actin was stained using Phalloidin-Tetramethylrhodamine B-Isothiocyanate (Sigma, P1951)
685 essentially as described before⁸². In brief, approximately 10^7 cells were harvested and fixed
686 with 3.7 % formaldehyde. Cells were washed in PEM buffer (100 mM PIPES, 5 mM EGTA, 5
687 mM MgCl_2 , pH 6.9) and stained with 50 $\mu\text{g/ml}$ final concentration of Phalloidin-TRITC in
688 PEM buffer with 25 % methanol. After washing cells were resuspended in PEM buffer
689 containing DAPI at a final concentration of 2.5 $\mu\text{g/ml}$ and mounted on agarose slides for
690 microscopy.

691 Nuclear staining of live cells in Fig. 5A was performed using Hoechst (bisbenzimidazole H 33342).
692 Cell wall staining for chitin exposure was performed using calcofluor white fluorescent
693 brightener (Sigma, 910090) at a final concentration of 100 $\mu\text{g/ml}$ ⁸³.

694 The vacuole morphology was visualised by staining with SynaptoRed(TM) C2 (equivalent to
695 FM4-64; Biotum BOT-70021) as described before⁸⁴.

696 Rhodamine B hexylester perchlorate (Molecular Probes, Y-7530) was used at a final
697 concentration of 100 nM to stain functional mitochondria. Pearson colocalisation coefficients
698 for Slt2-GFP colocalization with Rhodamine B hexylester signal were determined in Huyghens
699 essential 21.10 using the colocalization analyzer wizard with Gaussian minimum estimation.

700 Lipid droplets were stained with Bodipy 493/503 or autodot. Bodipy was detected in the FITC
701 channel whereas autodot was detected in the DAPI channel. Quantification of lipid droplets
702 was performed after threshold setting with the “analyze particle” tool and total cell numbers
703 were counted with the “cell counter” plugin.

704

705 **RNA isolation and Microarray**

706 Total RNA was prepared from wild type and *act1-159* log phase cells from biological triplicate
707 cultures using a Qiagen RNeasy kit including an on-column DNase digestion step according
708 to the manufacturer’s instructions. Following reverse transcription reactions the cDNA
709 template was hybridised to an Affymetrix Yeast 2.0 GeneChip array. Data was quality
710 controlled and normalised using the Bioconductor plugin, affylmGUI⁸⁵. To reduce background
711 noise we used the Robust Multi-Array Average (RMA) algorithm⁸⁶. The affylmGUI package
712 was run using R (version 3.1.0) to generate volcano plots. A significance threshold value for
713 95% odds of differential expression was chosen, which corresponds to a B statistic of 2.94
714 and above. We then sorted the significant data into groups for processing using Gene Ontology
715 (GO) Slim Mapper and Yeastmine⁸⁷ analysis tools from SGD⁷⁰.

716

717 **Immunoblotting**

718 For Western blot analysis, cell equivalents of an OD₆₀₀ of 3 were harvested at 24 h after
719 inoculation, and cell extracts were obtained from chemical lysis as described in⁸⁸. Proteins were
720 collected by centrifugation and resuspended in 75 µL 1× loading buffer (125 mM Tris-HCl,
721 adjusted to pH 6.8; 20% glycerol; 3% SDS; 2% DTT; 0.1% bromophenol blue), and heated to
722 95 °C for 10 min. Samples were centrifuged at 13,000 rpm for 12 s and 10 µL or 15 µL of the
723 supernatant was used for standard SDS-PAGE. Immunoblotting followed standard procedures,
724 with transfer of proteins to a 0.45 µm nitrocellulose membrane and probing with antibodies
725 against phospho-Slt2 (Phospho-p44/42 MAPK, cell signalling, #9101, 1:1000), actin (α -Yeast
726 act1 Goat monoclonal antibody, a kind gift from Prof. John Cooper, Washington University,
727 1:2000), (glyceraldehyde-3-phosphate dehydrogenase (GAPDH, Life Technologies,
728 MA515738, 1:5000), or VDAC/porin (Abcam, ab110326, 1:5000). As secondary antibodies,
729 we used IRDye goat anti-mouse (Licor, 926–68070, 1:20,000) or IRDye goat anti-rabbit (Licor,
730 928-40028, 1:20,000) as listed in the key resources table. Signals were recorded with Odyssey
731 Glx, with automatically determined exposure times. Quantitative analysis of western blots was
732 performed using image studio software.

733

734 **Lipid Extraction and Quantification by Shotgun Mass Spectrometry**

735 Yeast cultures were inoculated from stationary overnight cultures in YPD to fresh YPD medium
736 to an OD₆₀₀ of 0.1. In total, 2 OD₆₀₀ units were harvested after 24 h and homogenised with 0.5
737 mm zirconia beads in a cooled tissue lyser for 2 × 10 min at 30 Hz in 300 µL IPA. The whole
738 homogenate was evaporated in a vacuum desiccator to complete dryness. Lipid extraction was
739 performed according to^{89–91}. In brief, 700 µL internal standard mix in 10:3 MTBE/MeOH was
740 added to each sample and vortexed for 1 h at 4 °C. After the addition of 140 µL H₂O, samples
741 were vortexed for another 15 min. Phase separation was induced by centrifugation at 13,400
34

742 rpm for 15 min. The organic phase was transferred to a glass vial and evaporated. Samples were
743 reconstituted in 300 μ L 1:2 MeOH/CHCl₃. For lipidome, 5 μ L of sample were diluted with 95
744 μ L 4:2:1 IPA/MeOH/CHCl₃ + 7.5 mM ammonium formate.

745 Mass spectrometric analysis was performed on a Q Exactive instrument (Thermo Fisher
746 Scientific, Bremen, DE) equipped with a robotic nanoflow ion source TriVersa NanoMate
747 (Advion BioSciences, Ithaca, NY, USA) using nanoelectrospray chips with a diameter of 4.1
748 μ m. The ion source was controlled by the Chipsoft 8.3.1 software (Advion BioSciences).
749 Ionisation voltage was +0.96 kV in the positive and -0.96 kV in the negative mode; back
750 pressure was set at 1.25 psi in both modes. Samples were analysed by polarity switching⁹¹. The
751 temperature of the ion transfer capillary was 200 °C; S-lens RF level was set to 50%. Each
752 sample was analysed for 18 min. FT-MS spectra were acquired within the range of m/z 400–
753 1000 from 0 min to 0.2 min in the positive mode, and within the range of m/z 350–1200 from
754 6.2 min to 6.4 min in the negative mode at a mass resolution of R m/z 200 = 140,000, automated
755 gain control (AGC) of 3×10^6 , and with a maximal injection time of 3000 ms. Ergosterol was
756 determined by parallel reaction monitoring (PRM) FT-MS/MS between 0.2 and 1.7 min. For
757 FT-MS/MS, micro-scans were set to 1, isolation window to 0.8 Da, normalised collision energy
758 to 12.5%, AGC to 5×10^4 , and maximum injection time to 3000 ms. t-SIM in positive (1.7 to
759 6 min) and negative (6.4 to 18 min) mode was acquired with R @ m/z 200 = 140,000; automated
760 gain control of 5×10^4 ; maximum injection time of 650 ms; isolation window of 20 Th; and
761 scan range of m/z 400 to 1000 in positive and m/z 350 to 1200 in negative mode, respectively.

762 The inclusion list of masses targeted in t-SIM analyses started at m/z 355 in negative and m/z
763 405 in positive ion mode, and other masses were computed by adding 10 Th increment (i.e.,
764 m/z 355, 365, 375, ...) up to m/z 1005 in positive mode and up to m/z 1205 in negative mode.

765 All acquired spectra were filtered by PeakStrainer (<https://git.mpi-35>)

766 [cbg.de/labShevchenko/PeakStrainer/wikis/home](https://www.cbg.de/labShevchenko/PeakStrainer/wikis/home))⁹² and stitched together by an in-house-
767 developed script⁹³. Lipids were identified by LipidXplorer software⁹⁴. Molecular fragmentation
768 query language (MFQL) queries were compiled for ergosterol, ergosterol esters, PC, LPC, PE,
769 LPE, PI, LPI, PA, LPA, PG, LPG, PS, LPS, TG, DG, IPC, MIP2C, and MIPC lipid classes.
770 The identification relied on accurately determined intact lipid masses (mass accuracy better
771 than 5 ppm) and a signal-to-noise threshold higher than 3. Lipids were quantified by comparing
772 the isotopically corrected abundances of their molecular ions with the abundances of internal
773 standards of the same lipid class. Ergosterol, as well as ergosterol esters, were normalised to
774 the internal cholesterol and internal CE standard, respectively.

775

776 **Lipid Extraction and Quantification by Thin-Layer Chromatography**

777 Yeast cultures were inoculated from stationary overnight cultures in YPD to fresh YPD medium
778 to an OD₆₀₀ of 0.1. In total, 80 OD₆₀₀ units were harvested at 24 h after inoculation. Total
779 lipids were extracted with chloroform/methanol 2:1 (v/v) according to Folch et al. .
780 Cholesterylformate (Sigma, S448532) was added to each sample before extraction as an internal
781 standard. The organic phase was dried under a stream of nitrogen and dissolved in 1 mL of
782 chloroform/methanol (2:1, v/v). For neutral lipid separation a total of 40 µL of lipid extracts
783 was sprayed on HPTLC silica gel 60 plates, 20 x 10 cm (Merck, 1.05641.001) using a CAMAG
784 automatic TLC sampler (ATS4), whereas for phospholipid analysis only 20 µL were applied.
785 Lipid separation was performed using a CAMAG automatic developing chamber (ADC2).
786 Neutral lipids were separated with n-hexane, n-heptane, diethylether, acetic acid
787 (63/18.5/18.5/1 v/v) as mobile phase⁹⁶, whereas phospholipid separation was carried out using
788 CHCl₃/MeOH/water (32.5:12.5:2) mixture as mobile phase⁹⁷⁻⁹⁹. HPTLC plates were
789 derivatized with 0.01 % primuline applied in a CAMAG derivatizer followed by mild heating

36

790 to 40°C for 2 minutes on a CAMAG TLC plate heater 3. Developed HPTLC plates were imaged
791 using a CAMAG TLC visualizer 2 with VisionCATS software. Since peak separation of PI and
792 PS was not ideal in all samples we conducted an additional derivatisation step with ninhydrin
793 spray reagent (Sigma Aldrich, N1286), which only stains phospholipids containing free amino
794 groups and thus allows quantification of PS without PI. HPTLC bands were processed into
795 chromatograms and quantified by polynomial regression of standard curves calculated from the
796 applied standards. For phospholipids the standard contained 1- α -phosphatidylinositol
797 (840044P), phosphatidylcholine (16:0-18:1; 850457P), phosphatidylethanolamine (16:0-18:1;
798 850757P), phosphatidylserine (18:1-18:1; 840034P), cardiolipin (18:1-18:1; 710335P),
799 phosphatidic acid (16:0-18:1; 840101P) each at 500 ng/ μ l all purchased individually from
800 Sigma Aldrich. As a neutral lipid standard we either used a 1:10 dilution of the nonpolar lipid
801 mixture B from Matreya (#1130) which is an equal component mix of cholesteryl-oleate,
802 methyloleate, triolein, oleic acid, and cholesterol (each at 5 μ g/ μ l) additionally supplemented
803 with diacylglycerol (16:0-18:1; Sigma 800815O) or a custom-made neutral lipid standard
804 consisting of a mix of cholesteryl-oleate (700269P), cholesterylformate (S448532), triolein
805 (870110O), diacylglycerol (16:0-18:1; 800815O), oleic acid (O1008) all purchased individually
806 from Sigma Aldrich, and ergosterol from Thermofisher Scientific (117810050) each at 500
807 ng/ μ l. The standards were applied at increasing quantities from 250 ng to 15 μ g absolute mass.

808

809 **Electron microscopy high pressure freezing with a Leica EM HPM 100 and freeze** 810 **substitution**

811 Yeast strains were inoculated from a stationary overnight culture in YPD to an OD₆₀₀ of 0.1.
812 Cells were grown in YPD media and harvested at stationary phase after 24 h of growth and
813 immediately subjected to high pressure freezing. Cell pellets were loaded and frozen using 2000

814 bar under liquid nitrogen conditions within milliseconds. Freezing was followed by freeze
815 substitution in acetone by adding 2 % osmium tetroxide (OsO₄) and 0.2 % uranyl acetate (UAc)
816 at temperatures below -70°C. After substitution, the samples were embedded in TAAB (Agar
817 Scientific, Essex,GB) epoxy resin¹⁰⁰. High pressure frozen yeast cells were sectioned (70 nm)
818 with a UC7 Ultramicrotome (Leica Microsystems, Vienna, Austria) and stained with lead
819 citrate for 5 min and platinum blue¹⁰¹ for 15 min. Images were taken at 120 kV with a Tecnai
820 G2 FEI (Thermo Fisher Scientific) microscope equipped with an Ultrascan 1000 CCD Camera
821 (Gatan). Measurement of cell wall thickness on electron micrographs was performed in ImageJ
822 using the measure tool. For each strain condition at least 117 measurements of the inner and
823 outer cell wall at equally distributed loci around the cells were performed.

824 **QUANTIFICATION AND STATISTICAL ANALYSIS**

825 Statistical analyses were calculated in Graphpad Prism 8. Information on tests for significance
826 is given in each figure. Error bars indicate standard error of the mean (SEM) and asterisks in
827 the figures indicate significant differences, *p<0.05, **p<0.01, ***p<0.001, ****p<0.0001.

828

829 **References**

- 830 1. Mishra, M., Huang, J., and Balasubramanian, M.K. (2014). The yeast actin
831 cytoskeleton. *FEMS Microbiol. Rev.* 38, 213–227. 10.1111/1574-6976.12064.
- 832 2. Ren, W., Zhao, W., Cao, L., and Huang, J. (2021). Involvement of the Actin Machinery
833 in Programmed Cell Death. *Front. Cell Dev. Biol.* 8, 634849. 10.3389/fcell.2020.634849.
- 834 3. Bamburg, J.R., and Bernstein, B.W. (2008). ADF/Cofilin. *Curr. Biol.* 18, R273–R275.
835 10.1016/j.cub.2008.02.002.

- 836 4. Klamt, F., Zdanov, S., Levine, R.L., Pariser, A., Zhang, Y., Zhang, B., Yu, L.-R.,
837 Veenstra, T.D., and Shacter, E. (2009). Oxidant-induced apoptosis is mediated by oxidation of
838 the actin-regulatory protein cofilin. *Nat. Cell Biol.* *11*, 1241–1246. 10.1038/ncb1968.
- 839 5. Bamburg, J.R., and Wiggan, O.P. (2002). ADF/cofilin and actin dynamics in disease.
840 *Trends Cell Biol.* *12*, 598–605. 10.1016/S0962-8924(02)02404-2.
- 841 6. Kotiadis, V.N., Leadsham, J.E., Bastow, E.L., Gheeraert, A., Whybrew, J.M., Bard,
842 M., Lappalainen, P., and Gourlay, C.W. (2012). Identification of new surfaces of cofilin that
843 link mitochondrial function to the control of multi-drug resistance. *J. Cell Sci.* *125*, 2288–2299.
844 10.1242/jcs.099390.
- 845 7. Galluzzi, L., Vitale, I., Aaronson, S.A., Abrams, J.M., Adam, D., Agostinis, P.,
846 Alnemri, E.S., Altucci, L., Amelio, I., Andrews, D.W., et al. (2018). Molecular mechanisms of
847 cell death: recommendations of the Nomenclature Committee on Cell Death 2018. *Cell Death*
848 *Differ.* *25*, 486–541. 10.1038/s41418-017-0012-4.
- 849 8. Madeo, F., Fröhlich, E., and Fröhlich, K.-U. (1997). A Yeast Mutant Showing
850 Diagnostic Markers of Early and Late Apoptosis. *J. Cell Biol.* *139*, 729–734.
- 851 9. Büttner, S., Eisenberg, T., Herker, E., Carmona-Gutierrez, D., Kroemer, G., and
852 Madeo, F. (2006). Why yeast cells can undergo apoptosis: death in times of peace, love, and
853 war. *J. Cell Biol.* *175*, 521–525. 10.1083/jcb.200608098.
- 854 10. Carmona-Gutierrez, D., Bauer, M.A., Zimmermann, A., Aguilera, A., Austriaco, N.,
855 Ayscough, K., Balzan, R., Bar-Nun, S., Barrientos, A., Belenky, P., et al. (2018). Guidelines
856 and recommendations on yeast cell death nomenclature. *Microb. Cell* *5*, 4–31.
857 10.15698/mic2018.01.607.

- 858 11. Rockenfeller, P., Ring, J., Muschett, V., Beranek, A., Büttner, S., Carmona-Gutierrez,
859 D., Eisenberg, T., Khoury, C., Rechberger, G., Kohlwein, S.D., et al. (2010). Fatty acids trigger
860 mitochondrion-dependent necrosis. *Cell Cycle* 9, 2908–2914. 10.4161/cc.9.14.12346.
- 861 12. Rockenfeller, P., Smolnig, M., Diessl, J., Bashir, M., Schmiedhofer, V., Knittelfelder,
862 O., Ring, J., Franz, J., Foessler, I., Khan, M.J., et al. (2018). Diacylglycerol triggers Rim101
863 pathway-dependent necrosis in yeast: a model for lipotoxicity. *Cell Death Differ.* 25, 765.
864 10.1038/s41418-017-0014-2.
- 865 13. Rockenfeller, P., and Gourlay, C.W. (2018). Lipotoxicity in yeast: a focus on plasma
866 membrane signalling and membrane contact sites. *FEMS Yeast Res.* 18.
867 10.1093/femsyr/foy034.
- 868 14. Carmona-Gutierrez, D., Reisenbichler, A., Heimbucher, P., Bauer, M.A., Braun, R.J.,
869 Ruckenstuhl, C., Büttner, S., Eisenberg, T., Rockenfeller, P., Fröhlich, K.-U., et al. (2011).
870 Ceramide triggers metacaspase-independent mitochondrial cell death in yeast. *Cell Cycle*
871 *Georget. Tex* 10, 3973–3978. 10.4161/cc.10.22.18212.
- 872 15. Lappalainen, P., Fedorov, E.V., Fedorov, A.A., Almo, S.C., and Drubin, D.G. (1997).
873 Essential functions and actin-binding surfaces of yeast cofilin revealed by systematic
874 mutagenesis. *EMBO J.* 16, 5520–5530. 10.1093/emboj/16.18.5520.
- 875 16. González-Rubio, G., Sastre-Vergara, L., Molina, M., Martín, H., and Fernández-
876 Acero, T. (2022). Substrates of the MAPK Slt2: Shaping Yeast Cell Integrity. *J. Fungi* 8, 368.
877 10.3390/jof8040368.
- 878 17. Takasaki, T., Utsumi, R., Shimada, E., Bamba, A., Hagihara, K., Satoh, R., and
879 Sugiura, R. (2023). Atg1, a key regulator of autophagy, functions to promote MAPK activation
880 and cell death upon calcium overload in fission yeast. *Microb. Cell Graz Austria* 10, 133–140.
881 10.15698/mic2023.06.798.

- 882 18. Rego, A., Duarte, A.M., Azevedo, F., Sousa, M.J., Côrte-Real, M., and Chaves, S.R.
883 (2014). Cell wall dynamics modulate acetic acid-induced apoptotic cell death of
884 *Saccharomyces cerevisiae*. *Microb. Cell Graz Austria I*, 303–314. 10.15698/mic2014.09.164.
- 885 19. Kanda, Y., Satoh, R., Takasaki, T., Tomimoto, N., Tsuchiya, K., Tsai, C.A., Tanaka,
886 T., Kyomoto, S., Hamada, K., Fujiwara, T., et al. (2021). Sequestration of the PKC ortholog
887 Pck2 in stress granules as a feedback mechanism of MAPK signaling in fission yeast. *J. Cell*
888 *Sci.* 134, jcs250191. 10.1242/jcs.250191.
- 889 20. Illescas, M., Peñas, A., Arenas, J., Martín, M.A., and Ugalde, C. (2021). Regulation
890 of Mitochondrial Function by the Actin Cytoskeleton. *Front. Cell Dev. Biol.* 9, 795838.
891 10.3389/fcell.2021.795838.
- 892 21. Adams, A.E.M., and Pringle, J.R. (1984). Relationship of actin and tubulin distribution
893 to bud growth in wild- type and morphogenetic-mutant *Saccharomyces cerevisiae*. *J. Cell Biol.*
894 98, 934–945.
- 895 22. Kilmartin, J.V., and Adams, A.E.M. (1984). Structural rearrangements of tubulin and
896 actin during the cell cycle of the yeast *Saccharomyces*. *J. Cell Biol.* 98, 922–933.
- 897 23. Mulholland, J., Preuss, D., Moon, A., Wong, A., Drubin, D.G., and Botstein, D.
898 (1994). Ultrastructure of the yeast actin cytoskeleton and its association with the plasma
899 membrane. *J. Cell Biol.* 125, 381–391.
- 900 24. Novick, P., and Botstein, D. (1985). Phenotypic analysis of temperature-sensitive
901 yeast actin mutants. *Cell* 40. 10.1016/0092-8674(85)90154-0.
- 902 25. Lappalainen, P., and Drubin, D.G. (1997). Cofilin promotes rapid actin filament
903 turnover in vivo. *Nature* 388, 78–82. 10.1038/40418.

- 904 26. Kornmann, B., Currie, E., Collins, S.R., Schuldiner, M., Nunnari, J., Weissman, J.S.,
905 and Walter, P. (2009). An ER-Mitochondria Tethering Complex Revealed by a Synthetic
906 Biology Screen. *Science* 325, 477–481. 10.1126/science.1175088.
- 907 27. Soares, E. v. (2011). Flocculation in *Saccharomyces cerevisiae*: a review. *J. Appl.*
908 *Microbiol.* 110, 1–18. 10.1111/j.1365-2672.2010.04897.x.
- 909 28. Sariki, S.K., Kumawat, R., Singh, V., and Tomar, R.S. (2019). Flocculation of
910 *Saccharomyces cerevisiae* is dependent on activation of Slf2 and Rlm1 regulated by the cell
911 wall integrity pathway. *Mol. Microbiol.* 112, 1350–1369. 10.1111/mmi.14375.
- 912 29. Free, S.J. (2013). Chapter Two - Fungal Cell Wall Organization and Biosynthesis. In
913 *Advances in Genetics*, T. Friedmann, J. C. Dunlap, and S. F. Goodwin, eds. (Academic Press),
914 pp. 33–82. 10.1016/B978-0-12-407677-8.00002-6.
- 915 30. Levin, D.E. (2011). Regulation of Cell Wall Biogenesis in *Saccharomyces cerevisiae*:
916 The Cell Wall Integrity Signaling Pathway. *Genetics* 189, 1145–1175.
917 10.1534/genetics.111.128264.
- 918 31. Elorza, M.V., Rico, H., and Sentandreu, R. (1983). Calcofluor white alters the
919 assembly of chitin fibrils in *Saccharomyces cerevisiae* and *Candida albicans* cells. *J. Gen.*
920 *Microbiol.* 129, 1577–1582. 10.1099/00221287-129-5-1577.
- 921 32. Belmont, L.D., and Drubin, D.G. (1998). The Yeast V159N Actin Mutant Reveals
922 Roles for Actin Dynamics In Vivo. *J. Cell Biol.* 142, 1289–1299.
- 923 33. Lee, K.S., Irie, K., Gotoh, Y., Watanabe, Y., Araki, H., Nishida, E., Matsumoto, K.,
924 and Levin, D.E. (1993). A yeast mitogen-activated protein kinase homolog (Mpk1p) mediates
925 signalling by protein kinase C. *Mol. Cell. Biol.* 13, 3067–3075.

- 926 34. van Drogen, F., and Peter, M. (2002). Spa2p Functions as a Scaffold-like Protein to
927 Recruit the Mpk1p MAP Kinase Module to Sites of Polarized Growth. *Curr. Biol.* *12*, 1698–
928 1703. 10.1016/S0960-9822(02)01186-7.
- 929 35. Miyata, N., Fujii, S., and Kuge, O. (2018). Porin proteins have critical functions in
930 mitochondrial phospholipid metabolism in yeast. *J. Biol. Chem.* *293*, 17593–17605.
931 10.1074/jbc.RA118.005410.
- 932 36. Pfisterer, S.G., Gateva, G., Horvath, P., Pirhonen, J., Salo, V.T., Karhinen, L.,
933 Varjosalo, M., Ryhänen, S.J., Lappalainen, P., and Ikonen, E. (2017). Role for formin-like 1-
934 dependent acto-myosin assembly in lipid droplet dynamics and lipid storage. *Nat. Commun.* *8*.
935 10.1038/ncomms14858.
- 936 37. Weibel, G.L., Joshi, M.R., Jerome, W.G., Bates, S.R., Yu, K.J., Phillips, M.C., and
937 Rothblat, G.H. (2012). Cytoskeleton Disruption in J774 Macrophages: Consequences for Lipid
938 Droplet Formation and Cholesterol Flux. *Biochim. Biophys. Acta* *1821*, 464–472.
939 10.1016/j.bbalip.2011.09.015.
- 940 38. Yang, W., Thein, S., Wang, X., Bi, X., Ericksen, R.E., Xu, F., and Han, W. (2014).
941 BSCL2/seipin regulates adipogenesis through actin cytoskeleton remodelling. *Hum. Mol.*
942 *Genet.* *23*, 502–513. 10.1093/hmg/ddt444.
- 943 39. Choudhary, V., and Schneider, R. Lipid droplet biogenesis from specialized ER
944 subdomains. *Microb. Cell* *7*, 218–221. 10.15698/mic2020.08.727.
- 945 40. Lee, A.C., Xu, X., Blachly-Dyson, E., Forte, M., and Colombini, M. (1998). The role
946 of yeast VDAC genes on the permeability of the mitochondrial outer membrane. *J. Membr.*
947 *Biol.* *161*, 173–181.

- 948 41. Trindade, D., Pereira, C., Chaves, S.R., Manon, S., Côrte-Real, M., and Sousa, M.J.
949 (2016). VDAC regulates AAC-mediated apoptosis and cytochrome c release in yeast. *Microb.*
950 *Cell Graz Austria* 3, 500–510. 10.15698/mic2016.10.533.
- 951 42. Tulha, J., and Lucas, C. (2018). *Saccharomyces cerevisiae* mitochondrial
952 Por1/yVDAC1 (voltage-dependent anion channel 1) interacts physically with the MBOAT O-
953 acyltransferase Gup1/HHATL in the control of cell wall integrity and programmed cell death.
954 *FEMS Yeast Res.* 18, foy097. 10.1093/femsyr/foy097.
- 955 43. Bobba, A., Casalino, E., Amadoro, G., Petragallo, V.A., and Atlante, A. (2017).
956 AMPK is activated early in cerebellar granule cells undergoing apoptosis and influences
957 VADC1 phosphorylation status and activity. *Apoptosis* 22, 1069–1078. 10.1007/s10495-017-
958 1389-8.
- 959 44. Strogolova, V., Orlova, M., Shevade, A., and Kuchin, S. (2012). Mitochondrial Porin
960 Por1 and Its Homolog Por2 Contribute to the Positive Control of Snf1 Protein Kinase in
961 *Saccharomyces cerevisiae*. *Eukaryot. Cell* 11, 1568–1572. 10.1128/EC.00127-12.
- 962 45. Shevade, A., Strogolova, V., Orlova, M., Yeo, C.T., and Kuchin, S. (2018).
963 Mitochondrial Voltage-Dependent Anion Channel Protein Por1 Positively Regulates the
964 Nuclear Localization of *Saccharomyces cerevisiae* AMP-Activated Protein Kinase. *mSphere* 3,
965 e00482-17. 10.1128/mSphere.00482-17.
- 966 46. Waite, K.A., and Roelofs, J. (2022). Proteasome granule formation is regulated
967 through mitochondrial respiration and kinase signaling. *J. Cell Sci.*, jcs.259778.
968 10.1242/jcs.259778.
- 969 47. Vögtle, F.-N., Keller, M., Taskin, A.A., Horvath, S.E., Guan, X.L., Prinz, C.,
970 Opalińska, M., Zorzin, C., van der Laan, M., Wenk, M.R., et al. (2015). The fusogenic lipid

- 971 phosphatidic acid promotes the biogenesis of mitochondrial outer membrane protein Ugo1. J.
972 Cell Biol. 210, 951–960. 10.1083/jcb.201506085.
- 973 48. Zhong, Q., Li, G., Gvozdenovic-Jeremic, J., and Greenberg, M.L. (2007). Up-
974 regulation of the Cell Integrity Pathway in *Saccharomyces cerevisiae* Suppresses Temperature
975 Sensitivity of the *pgs1*Δ Mutant. J. Biol. Chem. 282, 15946–15953. 10.1074/jbc.M701055200.
- 976 49. Nunez, L.R., Jesch, S.A., Gaspar, M.L., Almaguer, C., Villa-Garcia, M., Ruiz-
977 Noriega, M., Patton-Vogt, J., and Henry, S.A. (2008). Cell Wall Integrity MAPK Pathway Is
978 Essential for Lipid Homeostasis. J. Biol. Chem. 283, 34204–34217. 10.1074/jbc.M806391200.
- 979 50. Shen, Z., Li, Y., Gasparski, A.N., Abeliovich, H., and Greenberg, M.L. (2017).
980 Cardiolipin regulates mitophagy through the PKC pathway. J. Biol. Chem., jbc.M116.753574.
981 10.1074/jbc.M116.753574.
- 982 51. Broeskamp, F., Edrich, E.S.M., Knittelfelder, O., Neuhaus, L., Meyer, T., Heyden, J.,
983 Habernig, L., Kreppel, F., Gourlay, C.W., and Rockenfeller, P. (2021). Porin 1 Modulates
984 Autophagy in Yeast. Cells 10, 2416. 10.3390/cells10092416.
- 985 52. Ellenrieder, L., Dieterle, M.P., Doan, K.N., Mårtensson, C.U., Floerchinger, A.,
986 Campo, M.L., Pfanner, N., and Becker, T. (2019). Dual Role of Mitochondrial Porin in
987 Metabolite Transport across the Outer Membrane and Protein Transfer to the Inner Membrane.
988 Mol. Cell 73, 1056-1065.e7. 10.1016/j.molcel.2018.12.014.
- 989 53. Martins, V.M., Fernandes, T.R., Lopes, D., Afonso, C.B., Domingues, M.R.M., Côte-
990 Real, M., and Sousa, M.J. (2019). Contacts in Death: The Role of the ER–Mitochondria Axis
991 in Acetic Acid-Induced Apoptosis in Yeast. J. Mol. Biol. 431, 273–288.
992 10.1016/j.jmb.2018.11.002.

- 993 54. Smethurst, D.G.J., and Cooper, K.F. (2017). ER fatalities-The role of ER-
994 mitochondrial contact sites in yeast life and death decisions. *Mech. Ageing Dev.* *161*, 225–233.
995 10.1016/j.mad.2016.07.007.
- 996 55. Zhong, Q., Gvozdenovic-Jeremic, J., Webster, P., Zhou, J., and Greenberg, M.L.
997 (2005). Loss of Function of KRE5 Suppresses Temperature Sensitivity of Mutants Lacking
998 Mitochondrial Anionic Lipids. *Mol. Biol. Cell* *16*, 665–675. 10.1091/mbc.E04-09-0808.
- 999 56. Dagley, M.J., Gentle, I.E., Beilharz, T.H., Pettolino, F.A., Djordjevic, J.T., Lo, T.L.,
1000 Uwamahoro, N., Rupasinghe, T., Tull, D.L., McConville, M., et al. (2011). Cell wall integrity
1001 is linked to mitochondria and phospholipid homeostasis in *Candida albicans* through the
1002 activity of the post-transcriptional regulator Ccr4-Pop2. *Mol. Microbiol.* *79*, 968–989.
1003 10.1111/j.1365-2958.2010.07503.x.
- 1004 57. Gatta, A.T., Wong, L.H., Sere, Y.Y., Calderón-Noreña, D.M., Cockcroft, S., Menon,
1005 A.K., and Levine, T.P. (2015). A new family of StART domain proteins at membrane contact
1006 sites has a role in ER-PM sterol transport. *eLife* *4*. 10.7554/eLife.07253.
- 1007 58. Quon, E., Nenadic, A., Zaman, M.F., Johansen, J., and Beh, C.T. (2022). ER-PM
1008 membrane contact site regulation by yeast ORPs and membrane stress pathways. *PLoS Genet.*
1009 *18*, e1010106. 10.1371/journal.pgen.1010106.
- 1010 59. Sokolov, S.S., Trushina, N.I., Severin, F.F., and Knorre, D.A. (2019). Ergosterol
1011 Turnover in Yeast: An Interplay between Biosynthesis and Transport. *Biochem. Mosc.* *84*, 346–
1012 357. 10.1134/S0006297919040023.
- 1013 60. Dey, P., Su, W.-M., Han, G.-S., and Carman, G.M. (2017). Phosphorylation of lipid
1014 metabolic enzymes by yeast protein kinase C requires phosphatidylserine and diacylglycerol.
1015 *J. Lipid Res.* *58*, 742–751. 10.1194/jlr.M075036.

- 1016 61. Su, W.-M., Han, G.-S., and Carman, G.M. (2014). Cross-talk Phosphorylations by
1017 Protein Kinase C and Pho85p-Pho80p Protein Kinase Regulate Pah1p Phosphatidate
1018 Phosphatase Abundance in *Saccharomyces cerevisiae*. *J. Biol. Chem.* 289, 18818–18830.
1019 10.1074/jbc.M114.581462.
- 1020 62. Hsieh, L.-S., Su, W.-M., Han, G.-S., and Carman, G.M. (2015). Phosphorylation
1021 Regulates the Ubiquitin-independent Degradation of Yeast Pah1 Phosphatidate Phosphatase by
1022 the 20S Proteasome. *J. Biol. Chem.* 290, 11467–11478. 10.1074/jbc.M115.648659.
- 1023 63. Park, Y., Han, G.-S., Mileykovskaya, E., Garrett, T.A., and Carman, G.M. (2015).
1024 Altered Lipid Synthesis by Lack of Yeast Pah1 Phosphatidate Phosphatase Reduces
1025 Chronological Life Span. *J. Biol. Chem.* 290, 25382. 10.1074/jbc.M115.680314.
- 1026 64. Sasser, T., Qiu, Q.-S., Karunakaran, S., Padolina, M., Reyes, A., Flood, B., Smith, S.,
1027 Gonzales, C., and Fratti, R.A. (2012). Yeast Lipin 1 Orthologue Pah1p Regulates Vacuole
1028 Homeostasis and Membrane Fusion. *J. Biol. Chem.* 287, 2221–2236.
1029 10.1074/jbc.M111.317420.
- 1030 65. van Meer, G., Voelker, D.R., and Feigenson, G.W. (2008). Membrane lipids: where
1031 they are and how they behave. *Nat. Rev. Mol. Cell Biol.* 9, 112–124. 10.1038/nrm2330.
- 1032 66. Mason, D.A., Shulga, N., Undavai, S., Ferrando-May, E., Rexach, M.F., and Goldfarb,
1033 D.S. (2005). Increased nuclear envelope permeability and Pep4p-dependent degradation of
1034 nucleoporins during hydrogen peroxide-induced cell death. *FEMS Yeast Res.* 5, 1237–1251.
1035 10.1016/j.femsyr.2005.07.008.
- 1036 67. Sousa, M.J., Azevedo, F., Pedras, A., Marques, C., Coutinho, O.P., Preto, A., Gerós,
1037 H., Chaves, S.R., and Côrte-Real, M. (2011). Vacuole-mitochondrial cross-talk during
1038 apoptosis in yeast: a model for understanding lysosome-mitochondria-mediated apoptosis in
1039 mammals. *Biochem. Soc. Trans.* 39, 1533–1537. 10.1042/BST0391533.

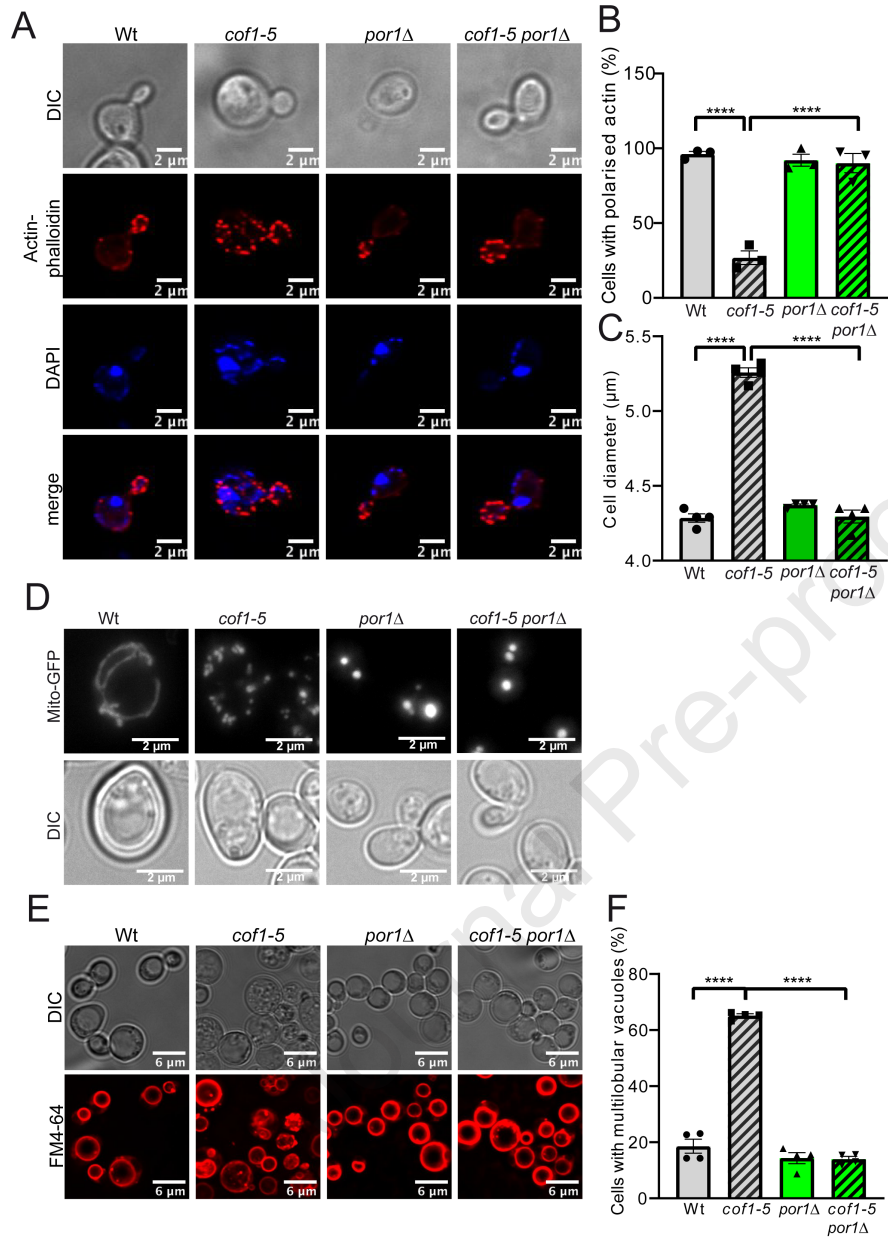
- 1040 68. Pereira, C., Chaves, S., Alves, S., Salin, B., Camougrand, N., Manon, S., Sousa, M.J.,
1041 and Côte-Real, M. (2010). Mitochondrial degradation in acetic acid-induced yeast apoptosis:
1042 the role of Pep4 and the ADP/ATP carrier. *Mol. Microbiol.* *76*, 1398–1410. 10.1111/j.1365-
1043 2958.2010.07122.x.
- 1044 69. Stolp, Z.D., Kulkarni, M., Liu, Y., Zhu, C., Jalisi, A., Lin, S., Casadevall, A.,
1045 Cunningham, K.W., Pineda, F.J., Teng, X., et al. (2022). Yeast cell death pathway requiring
1046 AP-3 vesicle trafficking leads to vacuole/lysosome membrane permeabilization. *Cell Rep.* *39*.
1047 10.1016/j.celrep.2022.110647.
- 1048 70. Cherry, J.M., Hong, E.L., Amundsen, C., Balakrishnan, R., Binkley, G., Chan, E.T.,
1049 Christie, K.R., Costanzo, M.C., Dwight, S.S., Engel, S.R., et al. (2012). *Saccharomyces*
1050 Genome Database: the genomics resource of budding yeast. *Nucleic Acids Res.* *40*, D700–
1051 D705. 10.1093/nar/gkr1029.
- 1052 71. Guldener, U. (1996). A new efficient gene disruption cassette for repeated use in
1053 budding yeast. *Nucleic Acids Res.* *24*, 2519–2524. 10.1093/nar/24.13.2519.
- 1054 72. Houseley, J., and Tollervey, D. (2011). Repeat expansion in the budding yeast
1055 ribosomal DNA can occur independently of the canonical homologous recombination
1056 machinery. *Nucleic Acids Res.* *39*, 8778–8791. 10.1093/nar/gkr589.
- 1057 73. Janke, C., Magiera, M.M., Rathfelder, N., Taxis, C., Reber, S., Maekawa, H., Moreno-
1058 Borchart, A., Doenges, G., Schwob, E., Schiebel, E., et al. (2004). A versatile toolbox for PCR-
1059 based tagging of yeast genes: new fluorescent proteins, more markers and promoter substitution
1060 cassettes. *Yeast* *21*, 947–962. 10.1002/yea.1142.
- 1061 74. Bähler, J., Wu, J.-Q., Longtine, M.S., Shah, N.G., Iii, A.M., Steever, A.B., Wach, A.,
1062 Philippsen, P., and Pringle, J.R. (1998). Heterologous modules for efficient and versatile PCR-

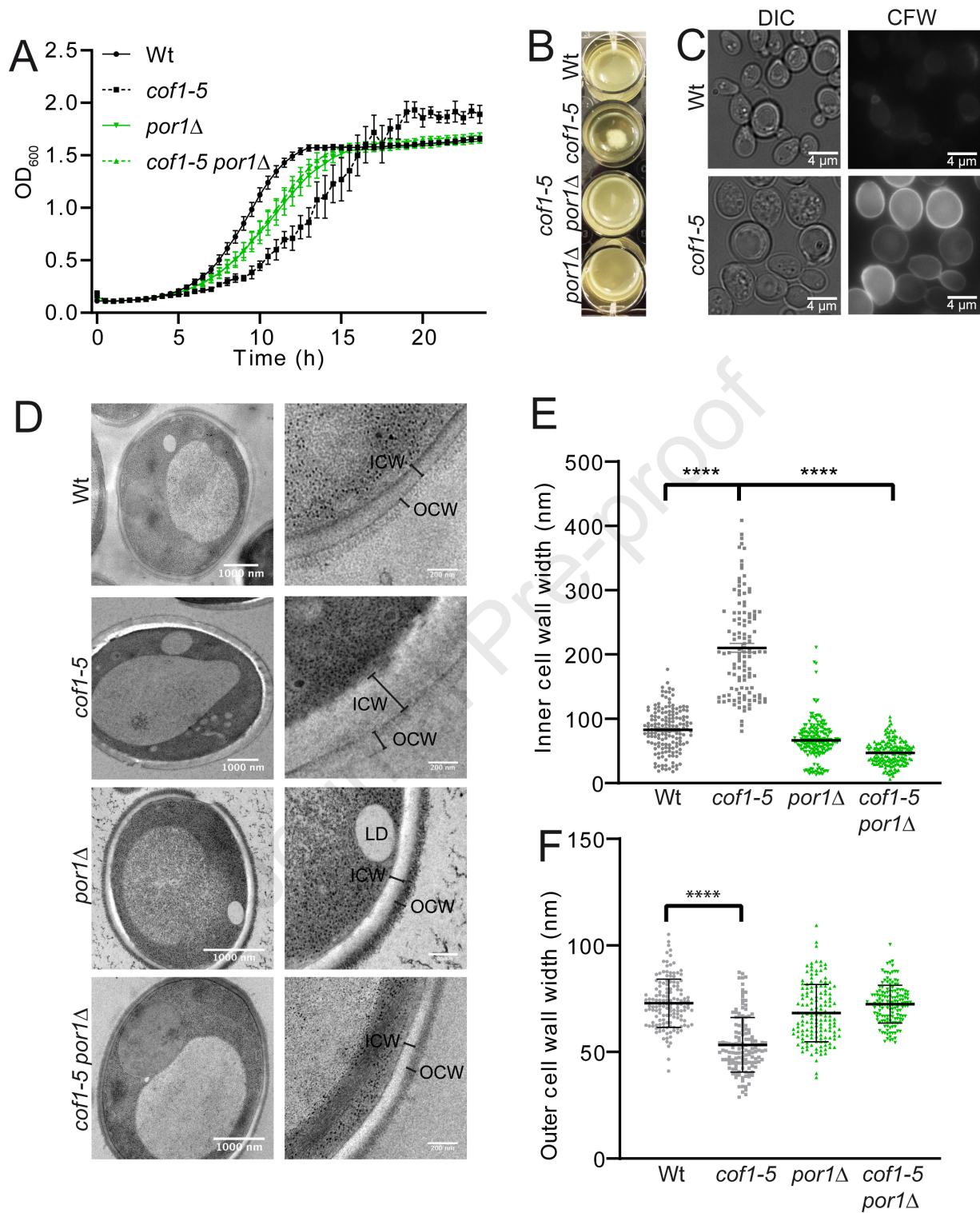
- 1063 based gene targeting in *Schizosaccharomyces pombe*. *Yeast* *14*, 943–951. 10.1002/(SICI)1097-
1064 0061(199807)14:10<943::AID-YEA292>3.0.CO;2-Y.
- 1065 75. Alberti, S., Gitler, A.D., and Lindquist, S. (2007). A suite of Gateway® cloning
1066 vectors for high-throughput genetic analysis in *Saccharomyces cerevisiae*. *Yeast* Chichester
1067 Engl. *24*, 913–919. 10.1002/yea.1502.
- 1068 76. Westermann, B., and Neupert, W. (2000). Mitochondria-targeted green fluorescent
1069 proteins: convenient tools for the study of organelle biogenesis in *Saccharomyces cerevisiae*.
1070 *Yeast* *16*, 1421–1427. 10.1002/1097-0061(200011)16:15<1421::AID-YEA624>3.0.CO;2-U.
- 1071 77. Daniel Gietz, R., and Woods, R.A. (2002). Transformation of yeast by lithium
1072 acetate/single-stranded carrier DNA/polyethylene glycol method. In *Methods in Enzymology*
1073 *Guide to Yeast Genetics and Molecular and Cell Biology - Part B.*, C. Guthrie and G. R. Fink,
1074 eds. (Academic Press), pp. 87–96. 10.1016/S0076-6879(02)50957-5.
- 1075 78. Kainz, K., Tadic, J., Zimmermann, A., Pendl, T., Carmona-Gutierrez, D., Ruckstuhl,
1076 C., Eisenberg, T., and Madeo, F. (2017). Chapter Nineteen - Methods to Assess Autophagy and
1077 Chronological Aging in Yeast. In *Methods in Enzymology Molecular Characterization of*
1078 *Autophagic Responses, Part B.*, L. Galluzzi, J. M. Bravo-San Pedro, and G. Kroemer, eds.
1079 (Academic Press), pp. 367–394. 10.1016/bs.mie.2016.09.086.
- 1080 79. Eisenberg, T., Carmona-Gutierrez, D., Büttner, S., Tavernarakis, N., and Madeo, F.
1081 (2010). Necrosis in yeast. *Apoptosis* *15*, 257–268. 10.1007/s10495-009-0453-4.
- 1082 80. Wolinski, H., Bredies, K., and Kohlwein, S.D. (2012). Quantitative imaging of lipid
1083 metabolism in yeast: from 4D analysis to high content screens of mutant libraries. *Methods Cell*
1084 *Biol.* *108*, 345–365. 10.1016/B978-0-12-386487-1.00016-X.

- 1085 81. Schindelin, J., Arganda-Carreras, I., Frise, E., Kaynig, V., Longair, M., Pietzsch, T.,
1086 Preibisch, S., Rueden, C., Saalfeld, S., Schmid, B., et al. (2012). Fiji - an Open Source platform
1087 for biological image analysis. *Nat. Methods* 9. 10.1038/nmeth.2019.
- 1088 82. Hasek, J. (2006). Yeast fluorescence microscopy. *Methods Mol. Biol. Clifton NJ* 313,
1089 85–96. 10.1385/1-59259-958-3:085.
- 1090 83. Pringle, J.R. (1991). [52] Staining of bud scars and other cell wall chitin with
1091 Calcofluor. In *Methods in Enzymology Guide to Yeast Genetics and Molecular Biology*.
1092 (Academic Press), pp. 732–735. 10.1016/0076-6879(91)94055-H.
- 1093 84. Vida, T.A., and Emr, S.D. (1995). A new vital stain for visualizing vacuolar membrane
1094 dynamics and endocytosis in yeast. *J. Cell Biol.* 128, 779–792.
- 1095 85. Wettenhall, J.M., Simpson, K.M., Satterley, K., and Smyth, G.K. (2006). affyImGUI:
1096 a graphical user interface for linear modeling of single channel microarray data. *Bioinformatics*
1097 22, 897–899. 10.1093/bioinformatics/btl025.
- 1098 86. Bolstad, B.M., Irizarry, R.A., Åstrand, M., and Speed, T.P. (2003). A comparison of
1099 normalization methods for high density oligonucleotide array data based on variance and bias.
1100 *Bioinformatics* 19, 185–193. 10.1093/bioinformatics/19.2.185.
- 1101 87. Balakrishnan, R., Park, J., Karra, K., Hitz, B.C., Binkley, G., Hong, E.L., Sullivan, J.,
1102 Micklem, G., and Cherry, J.M. (2012). YeastMine--an integrated data warehouse for
1103 *Saccharomyces cerevisiae* data as a multipurpose tool-kit. *Database J. Biol. Databases Curation*
1104 2012, bar062. 10.1093/database/bar062.
- 1105 88. Riezman, H., Hase, T., van Loon, A.P., Grivell, L.A., Suda, K., and Schatz, G. (1983).
1106 Import of proteins into mitochondria: a 70 kilodalton outer membrane protein with a large
1107 carboxy-terminal deletion is still transported to the outer membrane. *EMBO J.* 2, 2161–2168.

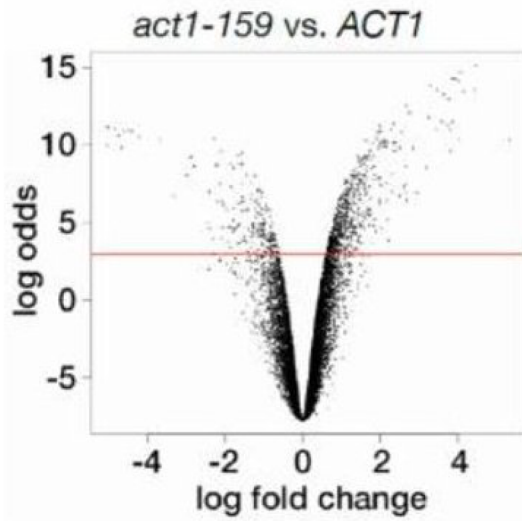
- 1108 89. Sales, S., Knittelfelder, O., and Shevchenko, A. (2017). Lipidomics of Human Blood
1109 Plasma by High-Resolution Shotgun Mass Spectrometry. *Methods Mol. Biol. Clifton NJ* 1619,
1110 203–212. 10.1007/978-1-4939-7057-5_16.
- 1111 90. Sales, S., Graessler, J., Ciucci, S., Al-Atrib, R., Vihervaara, T., Schuhmann, K.,
1112 Kauhanen, D., Sysi-Aho, M., Bornstein, S.R., Bickle, M., et al. (2016). Gender, Contraceptives
1113 and Individual Metabolic Predisposition Shape a Healthy Plasma Lipidome. *Sci. Rep.* 6.
1114 10.1038/srep27710.
- 1115 91. Schuhmann, K., Almeida, R., Baumert, M., Herzog, R., Bornstein, S.R., and
1116 Shevchenko, A. (2012). Shotgun lipidomics on a LTQ Orbitrap mass spectrometer by
1117 successive switching between acquisition polarity modes. *J. Mass Spectrom. JMS* 47, 96–104.
1118 10.1002/jms.2031.
- 1119 92. Schuhmann, K., Thomas, H., Ackerman, J.M., Nagornov, K.O., Tsybin, Y.O., and
1120 Shevchenko, A. (2017). Intensity-Independent Noise Filtering in FT MS and FT MS/MS
1121 Spectra for Shotgun Lipidomics. *Anal. Chem.* 89, 7046–7052. 10.1021/acs.analchem.7b00794.
- 1122 93. Schuhmann, K., Srzentić, K., Nagornov, K.O., Thomas, H., Gutmann, T., Coskun, Ü.,
1123 Tsybin, Y.O., and Shevchenko, A. (2017). Monitoring Membrane Lipidome Turnover by
1124 Metabolic ¹⁵N Labeling and Shotgun Ultra-High-Resolution Orbitrap Fourier Transform Mass
1125 Spectrometry. *Anal. Chem.* 89, 12857–12865. 10.1021/acs.analchem.7b03437.
- 1126 94. Herzog, R., Schuhmann, K., Schwudke, D., Sampaio, J.L., Bornstein, S.R., Schroeder,
1127 M., and Shevchenko, A. (2012). LipidXplorer: A Software for Consensual Cross-Platform
1128 Lipidomics. *PLoS ONE* 7. 10.1371/journal.pone.0029851.
- 1129 95. Folch, J., Lees, M., and Stanley, G.H.S. (1957). A Simple Method for the Isolation and
1130 Purification of Total Lipides from Animal Tissues. *J. Biol. Chem.* 226, 497–509.

- 1131 96. Schmitz, G., Assmann, G., and Bowyer, D.E. (1984). A quantitative densitometric
1132 method for the rapid separation and quantitation of the major tissue and lipoprotein lipids by
1133 high-performance thin-layer chromatography: I. Sample preparation, chromatography, and
1134 densitometry. *J. Chromatogr. B. Biomed. Sci. App.* 307, 65–79. 10.1016/S0378-
1135 4347(00)84073-6.
- 1136 97. Schneiter, R., and Daum, G. (2006). Analysis of yeast lipids. *Methods Mol. Biol.*
1137 Clifton NJ 313, 75–84. 10.1385/1-59259-958-3:075.
- 1138 98. Mangold, H.K. (1961). Thin-layer chromatography of lipids. *J. Am. Oil Chem. Soc.*
1139 38, 708–727. <https://doi.org/10.1007/BF02633061>.
- 1140 99. Knittelfelder, O.L., and Kohlwein, S.D. (2017). Thin-Layer Chromatography to
1141 Separate Phospholipids and Neutral Lipids from Yeast. *Cold Spring Harb. Protoc.* 2017.
1142 10.1101/pdb.prot085456.
- 1143 100. Kolb, D., Pritz, E., Steinecker-Frohnwieser, B., Lohberger, B., Deutsch, A., Kroneis,
1144 T., El-Heliebi, A., Dohr, G., Meditz, K., Wagner, K., et al. (2014). Extended Ultrastructural
1145 Characterization of Chordoma Cells: The Link to New Therapeutic Options. *PLoS ONE* 9,
1146 e114251. 10.1371/journal.pone.0114251.
- 1147 101. Inaga, S., Katsumoto, T., Tanaka, K., Kameie, T., Nakane, H., and Naguro, T. (2007).
1148 Platinum blue as an alternative to uranyl acetate for staining in transmission electron
1149 microscopy. *Arch. Histol. Cytol.* 70, 43–49. 10.1679/aohc.70.43.
- 1150

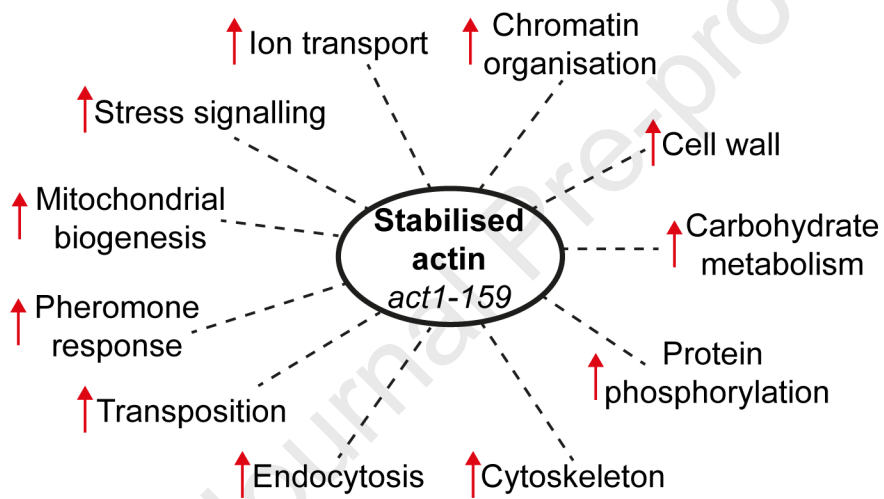




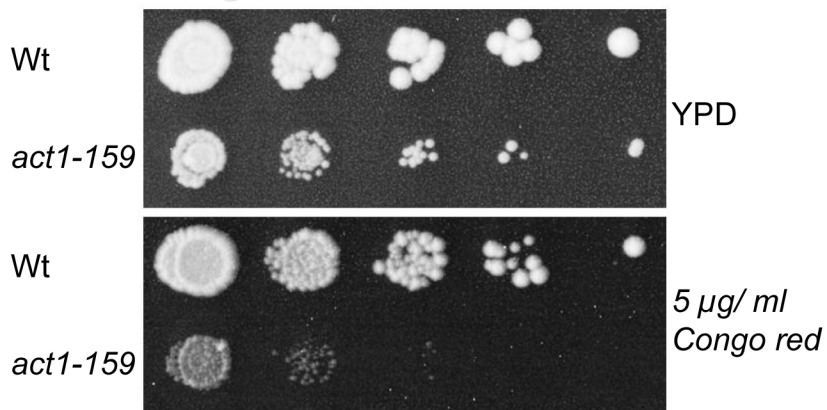
A

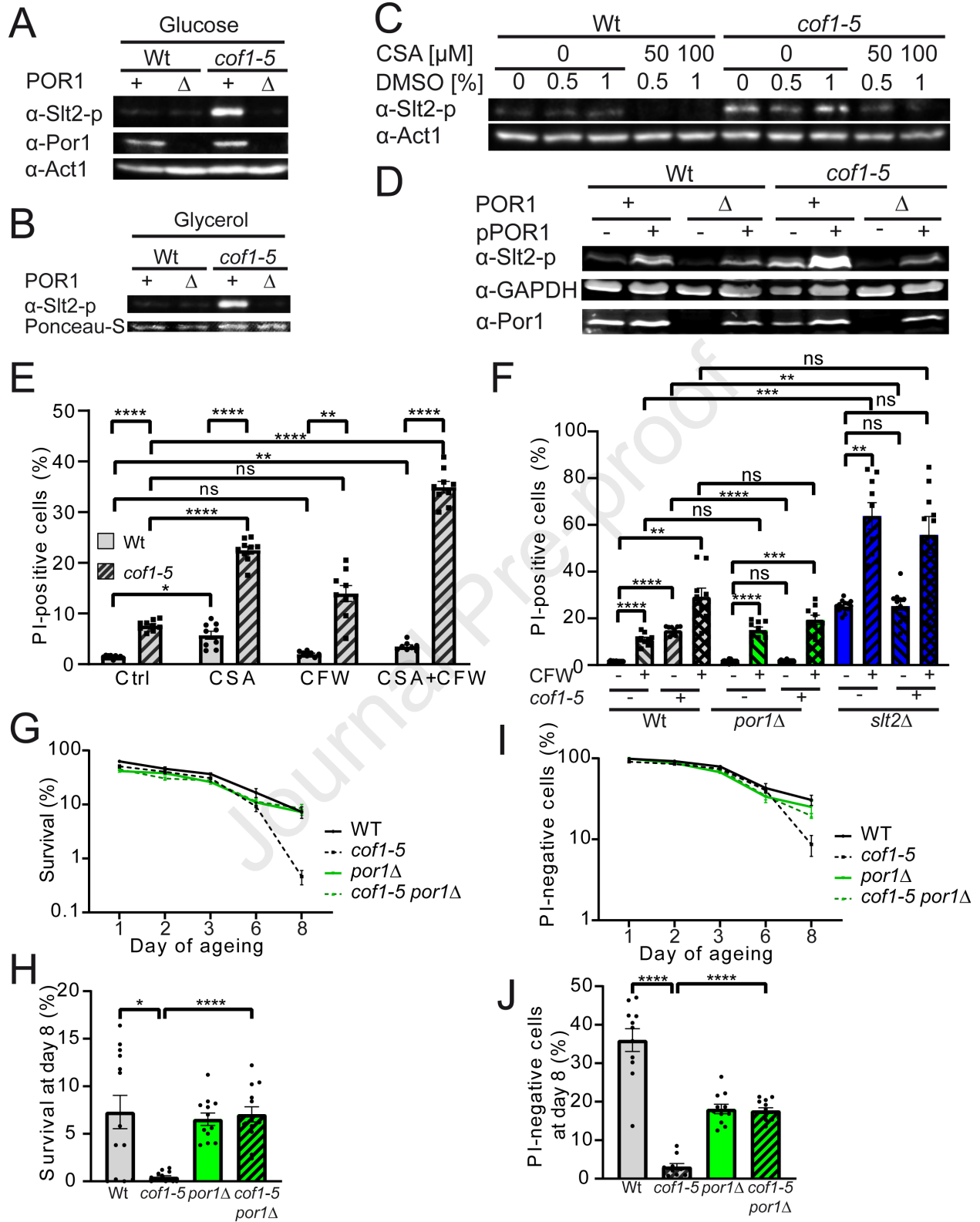


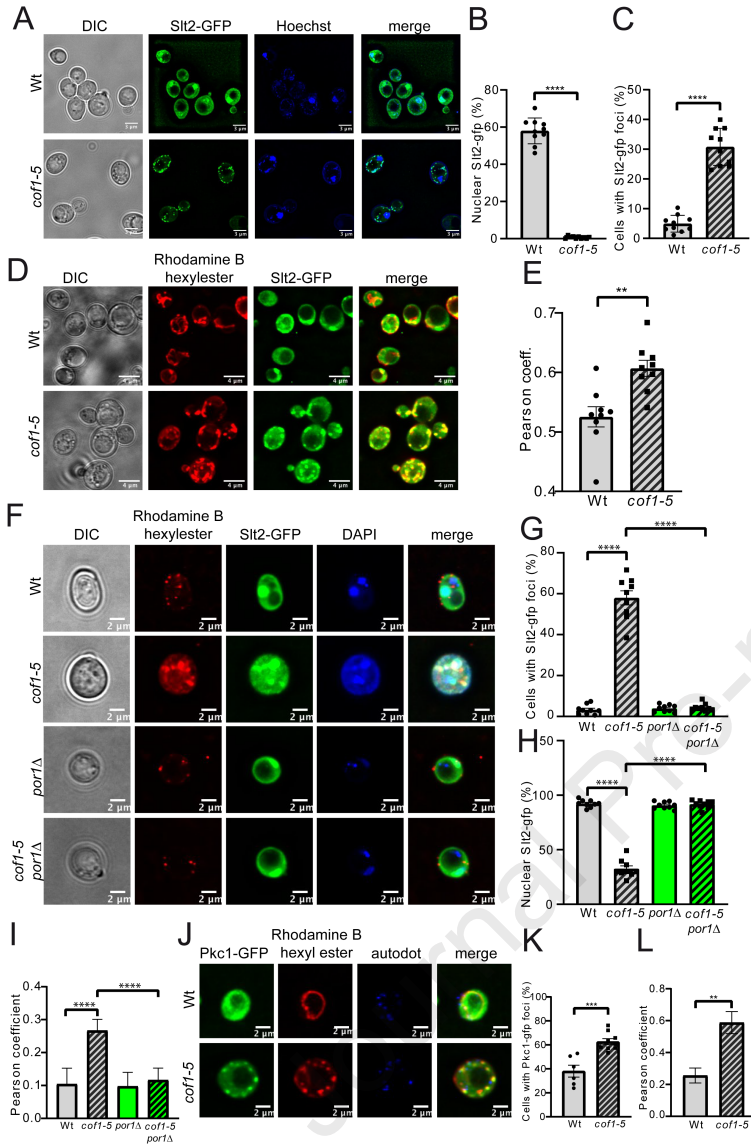
B

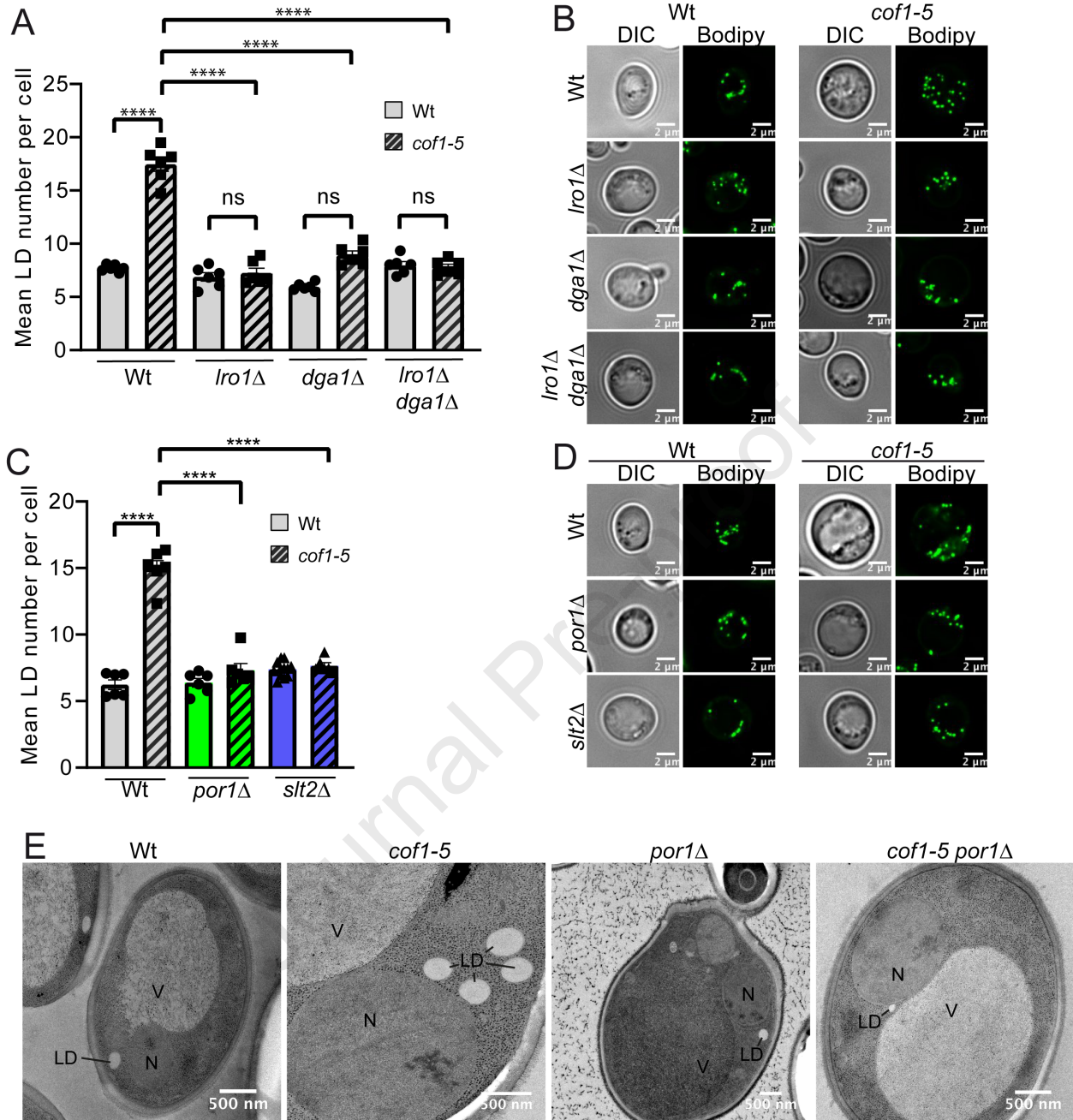


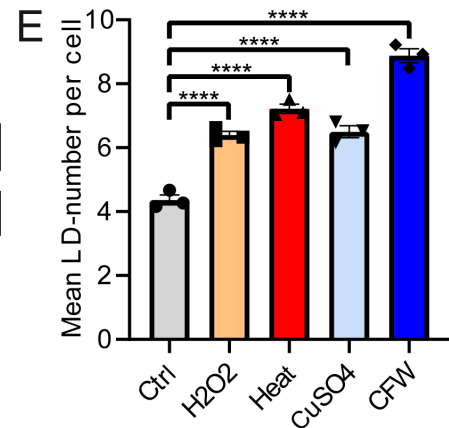
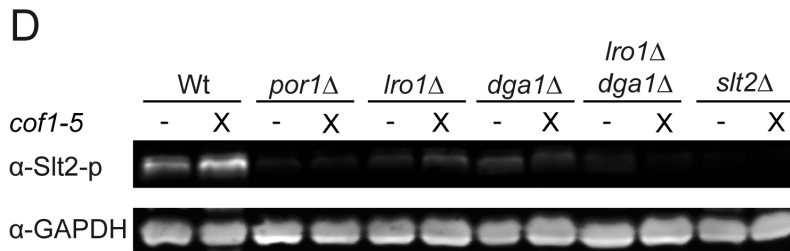
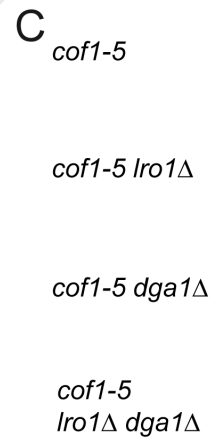
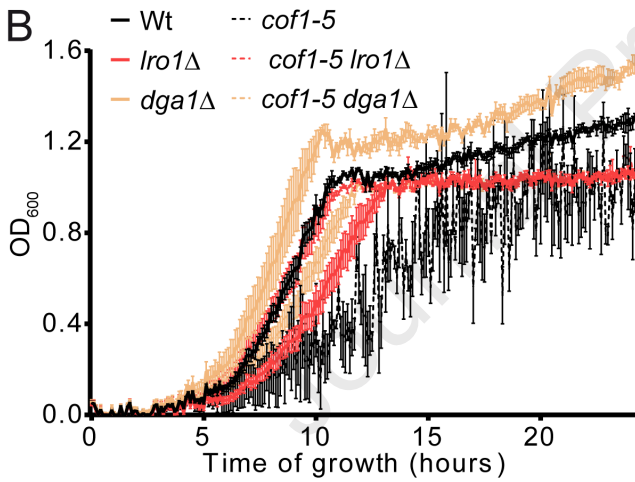
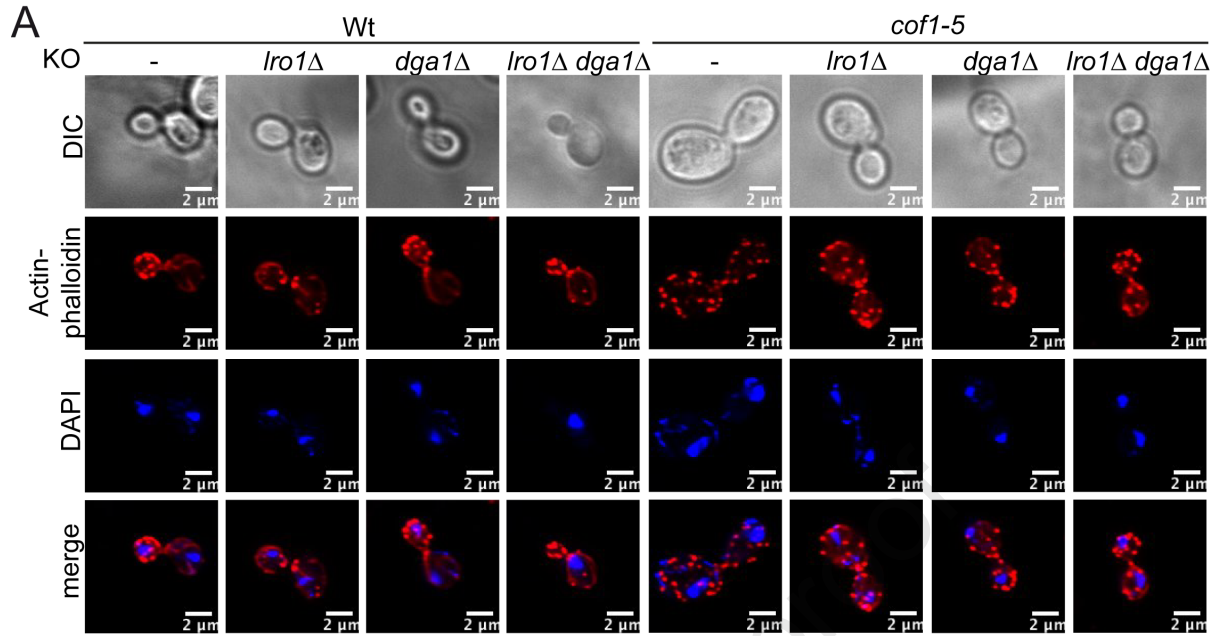
C

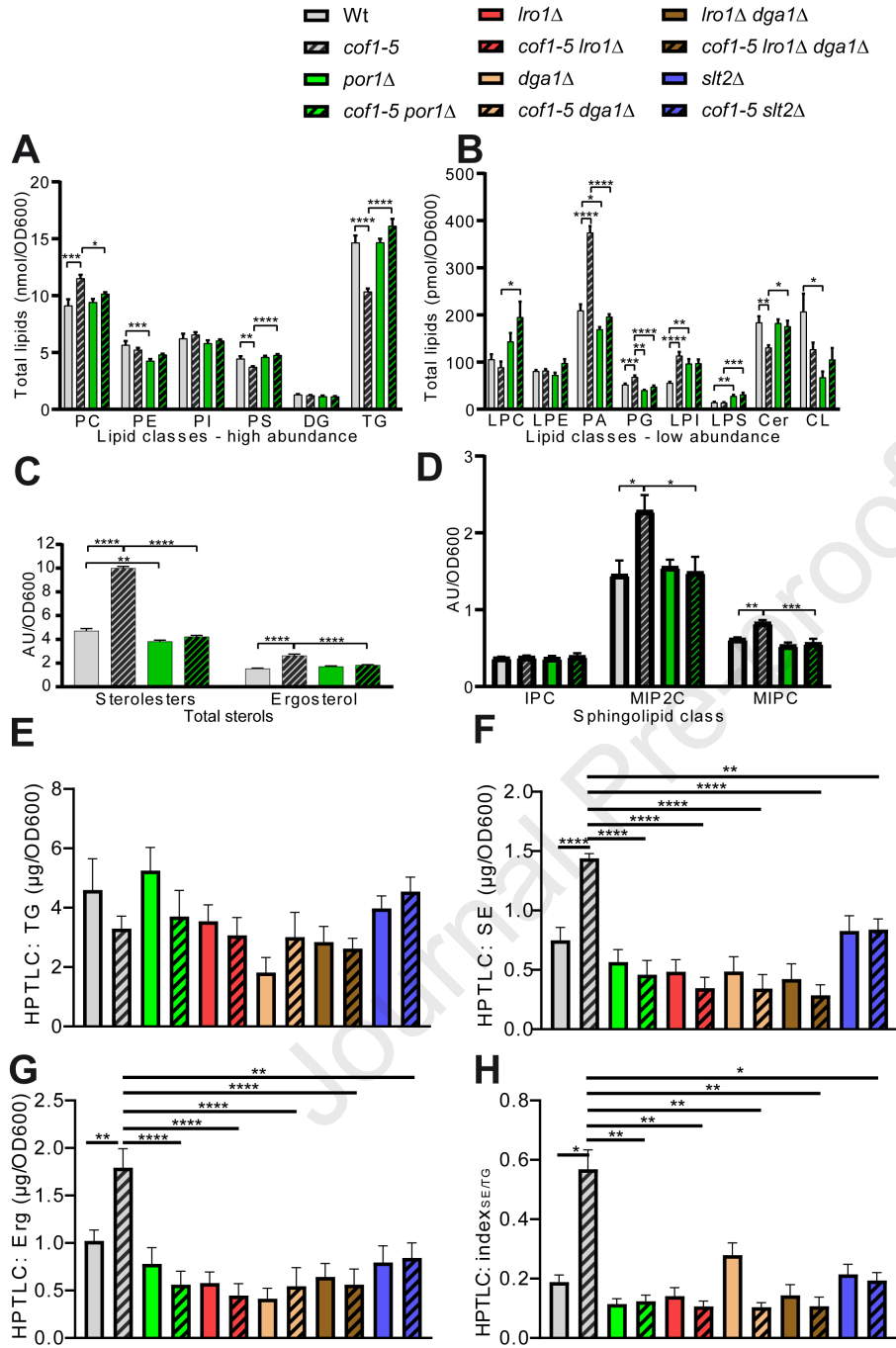












Highlights

- 1) *cof1-5* mutation activates CWI-signalling in a VDAC-dependent manner.
- 2) *cof1-5* expression promotes MAPK signalling from the mitochondrial compartment.
- 3) Cofilin and VDAC/ Porin are important regulators of lipid homeostasis.

Journal Pre-proof

Key resources table

REAGENT or RESOURCE	SOURCE	IDENTIFIER
Antibodies		
α -Phospho-p44/42 MAPK	cell signalling	#9101
α -Yeast act1 Goat monoclonal antibody	John Cooper	n/a
α -GAPDH	Life Technologies	MA515738
α -VDAC/porin	Abcam	ab110326
IRDye goat anti-mouse	Licor	#926-68070
IRDye goat anti-rabbit	Licor	#928-40028
Bacterial and virus strains		
pYX122-mtGFP	B. Westermann ⁷⁶	pCG44
pRS426-SLT2-GFP	Matthias Peter ³⁴	PPR A75
pAG418-POR1	This study	YPR B06
pDONR221- <i>POR1</i>	DNASU	FLH201444.01X
pFA6a-KanMX6	Addgene.org ⁷⁴	#39296; PPR C31
pFA6a-Ura3	Addgene.org ⁷²	#61924; PPR C29
pYM27	EUROSCARF ⁷³	YPR B35
Chemicals, peptides, and recombinant proteins		
Cercosporamide (CSA)	Sigma-Aldrich	SML0172
Calcofluor white (CFW)	Sigma-Aldrich	910090
Phalloidin-Tetramethylrhodamine B-Isothiocyanate	Sigma-Aldrich	P1951
SynaptoRed™ C2 (equivalent to FM4-64)	Biotum	BOT-70021
Rhodamine B hexylester perchlorate	Molecular Probes	Y-7530
Bodipy 493/503	Sigma-Aldrich	#490389
Autodot	Abcepta	# SM1000a
Critical commercial assays		
RNAeasy kit	Qiagen	#74004
Yeast 2.0 GeneChip array	Affymetrix	#900553
Deposited data		
Raw and analyzed data	This paper, Mendeley Data	10.17632/bgkscw9ns9.1
Microarray	This paper; Mendeley Data	10.17632/bgkscw9ns9.1
Shotgun lipidomics	This paper; Mendeley Data	10.17632/bgkscw9ns9.1
HPTLC lipidomics	This paper; Mendeley Data	10.17632/bgkscw9ns9.1
Experimental models: Organisms/strains		
<i>S. cerevisiae</i> : Strain background: BY4742 Mata <i>ura3-52 his3Δ200 leu2-3,112 lys2-801 ade2-101 COF1::LEU2</i>	Pekka Lappalainen ²⁵	YPR K43
<i>cof1-5 COF1::LEU2</i>	Pekka Lappalainen ²⁵	YPR K44
<i>por1Δ</i>	This paper	YPR K45
<i>cof1-5 por1Δ</i>	This paper	YPR K46
<i>lro1Δ</i>	This paper	YPR K62
<i>cof1-5 lro1Δ</i>	This paper	YPR K47
<i>dga1Δ</i>	This paper	YPR K63
<i>cof1-5 dga1Δ</i>	This paper	YPR K48
<i>lro1Δ dga1Δ</i>	This paper	YPR K64
<i>cof1-5 lro1Δ dga1Δ</i>	This paper	YPR K49

slt2Δ	This paper	YPR T29
cof1-5 slt2Δ	This paper	YPRT31
Wt SLT2-EGFP	This paper	YPR T12
cof1-5 SLT2-EGFP	This paper	YPR T15
<i>S. cerevisiae</i> : Strain background: BY4741 MATa ACT1::HIS3 his3D200 tub2-101 ura3-52 leu2-3, 112	David Drubin ³²	YPR K50
MATa act1-159::HIS3 his3D200 tub2-101 ura3-52 leu2-3, 112	David Drubin ³²	YPR K51
Oligonucleotides		
LRO1_fw:CCATTACAAAAGGTTCTCTACCAACGAATT CGGCGACAATCGAGTAAAAACAGCTGAAGCTTCGT ACGC	This paper	n/a
LRO1_rev:TTCGCTCTTTGAAATAATACACGGATGGA TAGTGAGTCAATGTCCGGTCATGCATAGGCCACTAGT GGATCTG	This paper	n/a
DGA1_fw:TACATATACATAAGGAAACGCAGAGGCAT ACAGTTTGAACAGTCAATAACAGCTGAAGCTTCGT ACGC	This paper	n/a
DGA1_rev:AAAATCCTTATTTATTCTAACATATTTGT GTTTTCCAATGAATTCATTAGCATAGGCCACTAGTG GATCTG	This paper	n/a
POR1-S1: CCAACACGAAACAGCCAAGCGTACCCAAAGCAAAA ATCAAACCAACCTCTCAACAAGTACGCTGCAGGTCTG AC	This paper	A80
POR1-S2: AAGAACGAGCACATATATGGTATATAGTGAACATAT ATATATTAGATATATACGTATCGATGAATTCGAGCTC G	This paper	A81
SLT2-S1: CTATCAAATAGTAGAAATAATTGAAGGGCGTGTAT AACAACTCTGGGAGATGCGTACGCTGCAGGTCTGAC	This paper	B40
SLT2-S2: CTTACATCTATGGTGAATTCTATACTTCCCCGGTTACT TATAGTTTTTTGTCCATAATCGATGAATTCGAGCTCG	This paper	B41
SLT2-S3: GCTTCTAGACCTTGAAAAAGAGCTGGAGTTTGGATT AGATAGAAAATATTTTCTGACGCTGCAGGTCTGAC	This paper	B42
PKC1-S2: CCGCTTAGATGTTTTATATAAAATTAATAAATCATG GCATGACCTTTTCTTCAATCGATGAATTCGAGCTCG	This paper	B45
PKC1-S3: GCCAGCAAGAAGAGTTTAGAGGATTTTCCTTTATGC CAGATGATTTGGATTTACGCTACGCTGCAGGTCTGAC	This paper	B46
Software and algorithms		
Fiji (ImageJ)	https://imagej.nih.gov/ij/ ⁸¹	n/a
GraphPad Prism 8.4.3	www.graphpad.com	n/a
R (3.1.0)	www.R-project.org	n/a
Slim Mapper	https://www.yeastgenome.org/goSlimMapper	n/a
Yeastmine	https://yeastmine.yeastgenome.org/yeastmine/begin.do ⁸⁷	n/a

Bioconductor plugin affyImgui	85	n/a
Robust Multi-Array Average (RMA) algorithm	86	n/a
PeakStrainer	https://git.mpi-cbg.de/labShevchenko/PeakStrainer/wikis/home ⁹²	n/a
LipidXplorer software	94	n/a
in-house-developed script	93	n/a
Other		
Resource website for yeast genetics SGD	https://www.yeastgenome.org ⁷⁰	n/a

Journal Pre-proof